ASTRONOMY & ASTROPHYSICS
SUPPLEMENT SERIES

Astron. Astrophys. Suppl. Ser. **119,** 333-367 (1996)

A 330−360 GHz spectral survey of G 34.3+0.15. I. Data and physical analysis⋆

G.H. Macdonald[1], A.G. Gibb[1], R.J. Habing[1] and T.J. Millar[2]

[1] Electronic Engineering Laboratory, University of Kent, Canterbury, Kent, CT2 7NT, UK
[2] Department of Physics, UMIST, P.O. Box 88, Manchester, M60 1QD, UK

Received June 9, 1995; accepted February 26, 1996

Abstract. — A 330−360 GHz spectral survey of the hot molecular core associated with the 'cometary' ultracompact HII region G 34.3+0.15 observed with the James Clerk Maxwell Telescope has detected 338 spectral lines from at least 35 distinct chemical species plus 19 isotopomers. 70 lines remain unidentified. Chemical abundance and rotation temperature have been determined by rotation diagram analysis for 12 species, and lower limits to abundance found for 38 others.

Key words: ISM: individual objects: G 34.3+0.15 — ISM: molecules — radio lines: ISM — Line: identification — ISM: abundances

1. Introduction

Millimetre- and submillimetre-wavelength spectral surveys of regions of massive star formation are beginning to yield valuable insights into the complex chemical processes occurring therein. As yet, sensitive spectral surveys have been performed over rather limited frequency ranges for very few regions, most notably OMC1 and Sgr B2 (Cummins et al. 1986; Johannson et al. 1984; Turner 1989; Sutton et al. 1985; Blake et al. 1986; Jewell et al. 1989). Turner (1991) has shown that, despite apparent differences in line intensities, the chemistry of both these hot molecular cores is essentially similar, suggesting a similar cosmic-ray flux, evolutionary stage and elemental abundance distribution. Whilst this result is striking for two star-forming regions of different size and location in the Galaxy, it may well be that such O-rich (O/C > 1) regions of massive star-formation with clumpy, complex morphologies are not typical of less evolved hot cores.

For this reason we have undertaken a spectral scan in the 330−360 GHz range, covering almost the whole of the 870 μm atmospheric window, of the hot core associated with the ultracompact HII region, G 34.3+0.15. Hot molecular cores are an important component of molecular clouds associated with sites of recent star formation. They may be defined as small (0.01−0.1 pc), warm (100−300 K), dense (10^6−10^8 cm^{-3}) and opaque ($N_{H_2} \simeq 10^{23}$−10^{24} cm^{-2}; A_V=100−1000 mag) clumps of gas with dynamical age, loosely defined as the ratio of hot core diameter to observed linewidth, of only a few thousand years. Since this is insufficient time for significant evolution to have occurred in the gas-phase chemistry, hot core abundances reflect conditions at the time of 'switch-on' of the exciting star which result in the evaporation of material from grain mantles due to direct heating or the effect of shocks (Walmsley 1992). The composition of the grain mantles in turn is a result of the production of molecules by gas-phase chemistry in the cold accreting cloud which have frozen onto the grain surface, and the subsequent processing of these species by surface chemistry. Study of the chemistry in hot molecular cores therefore provides valuable insight into the earlier cold phases of evolution of the star-forming molecular cloud.

The hot molecular core associated with the ultracompact HII region G 34.3+0.15 provides an excellent case study for the detailed investigation of the chemistry in an isolated hot core. The HII region is a prototypical example of the cometary morphology (Fig. 1), which may be due to the bow-shock interaction between an ambient molecular cloud and the wind from an energetic young star moving supersonically through the cloud (Wood & Churchwell 1989; Van Buren et al. 1990). NH_3(3,3) observations with the VLA (Heaton et al. 1989) show that the highly compact molecular cloud appears to be wrapped around the head of the cometary structure (Fig. 2), with the ionisation front advancing into the cloud. The distance to G 34.3+0.15 is taken to be 3.1 kpc.

Send offprint requests to: G.H. Macdonald
⋆Table 1 also available in electronic form at CDS via ftp 130.79.128.5

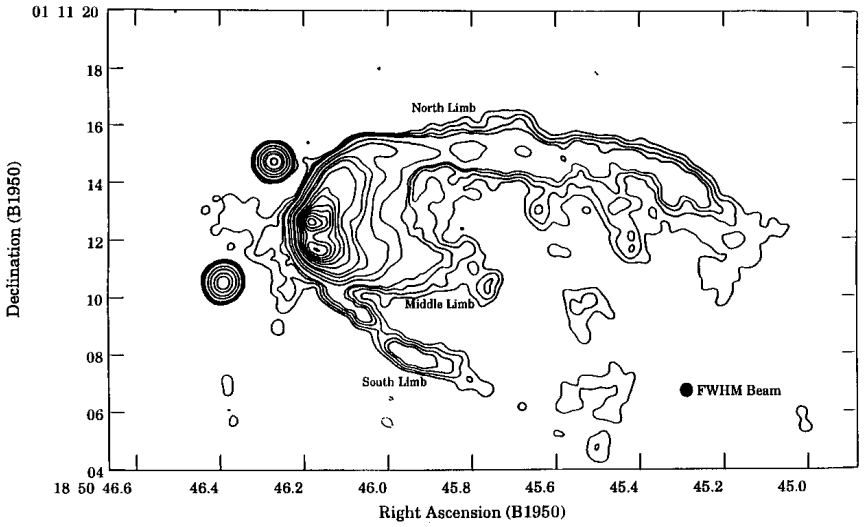

Fig. 1. VLA 15 GHz image of G 34.3+0.15 showing the 'cometary' structure of the ultracompact HII region (Gaume et al. 1994)

Radiative transfer modelling of continuum and spectral line emission from HCO^+ and CO are best fitted by a hierarchical structure with spherical symmetry comprising a halo, compact core and ultracompact core (Strong-Jones at al. 1991; Heaton et al. 1993; Little et al. 1994). In these models, the halo extends from $\sim 3.25-0.1$ pc with (to within a factor of ~ 2) $n_{\mathrm{H_2}} \simeq 10^4 r^{-2}\,\mathrm{cm}^{-3}$, $T_{\mathrm{K}} \simeq 30 r^{-0.4}\,\mathrm{K}$, where r is the radius in pc. The compact core extends from $\sim 0.1-0.01$ pc and has a constant density $n_{\mathrm{H_2}} \sim 10^6\,\mathrm{cm}^{-3}$ but otherwise as above. The ultracompact core represents the central region within $0.01-0.001$ pc and has constant density ($2\ 10^7\,\mathrm{cm}^{-3}$) and temperature ($\simeq 300$ K). In Paper II (Millar et al., in preparation) we will attempt to model the chemical abundances observed assuming this spherical structure.

The observations and method of data reduction will be described in Sect. 2, and determination of rotation temperature and chemical abundance for identified species discussed in Sect. 3. A detailed discussion of the significance of these new data in understanding the chemical evolution of hot molecular cores will be given in a subsequent paper (Paper II).

2. Observations and data reduction

2.1. *Observations*

The observations were made with the James Clerk Maxwell Telescope on four full nights in 1991 July (session 1) and six half-nights in 1992 March/April (session 2) with receiver B2, a dual channel Schottky diode mixer receiver with system temperature of typically 2000−3000 K. Data from only one channel were used since the other channel was considerably more noisy. The signal was analysed over a 500 MHz bandwidth with an acousto-optical spectrometer (AOSC) which provides 2048 frequency channels at 0.25 MHz spacing with resolution of 0.33 MHz.

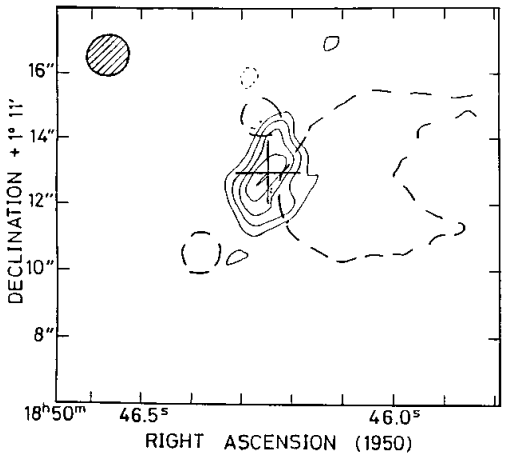

Fig. 2. VLA map of integrated $NH_3(3,3)$ hyperfine line emission from molecular core in G 34.3+0.15. Dashed line indicates cometary head of HII region (Heaton et al. 1989). JCMT beam centre position is shown with a cross

All data were calibrated by the standard chopper-wheel technique (Kutner & Ulich 1981), yielding line intensities of T_{A}^*, corrected for atmospheric and resistive losses in the telescope, plus rearward spillover and scattering. Further correction for forward spillover and scattering yields the quantity $T_{\mathrm{R}}^* = T_{\mathrm{A}}^*/\eta_{\mathrm{fss}}$, where the forward scattering and spillover efficiency $\eta_{\mathrm{fss}} = 0.75$ at 345 GHz for the JCMT. All spectra shown here are on the T_{A}^* scale. At 345 GHz, the half-power beamwidth is $14''$. Pointing was checked regularly using the submillimetre continuum emission of G 34.3+0.15 itself: pointing errors were found

to be less than 3″. All observations were made at the position $\alpha(1950) = 18^{\rm h}50^{\rm m}46\overset{\rm s}{.}25$, $\delta(1950) = +01°11'13''$; i.e. at the intersection of the ionisation front and the axis of symmetry of the cometary-shaped continuum emission (Fig. 2). A velocity of $+58\,{\rm km\,s^{-1}}$ with respect to the local standard of rest was assumed initially, although this was later revised to $+57.2\,{\rm km\,s^{-1}}$ (see Sect. 2.3).

Observations in the first session were made as a pilot programme over a total frequency range of 17 GHz with the 500 MHz bandwidth of AOSC centred at frequencies selected with reference to an earlier survey of Orion-KL (Jewell et al. 1989). Observations made in the second session covered the full frequency range from 330−360 GHz to provide data with a uniform noise level.

All observations were made in dual-sideband mode which gives rise to spectra in both upper- and lower- sidebands superimposed but with the frequency scales running in opposite directions. The sideband ambiguity was resolved for any given line by repeating each observation with the local oscillator frequency shifted by 10 MHz, causing lines observed in the two sidebands to move by this amount in opposing directions. Receiver B2 has an intermediate frequency of 3.94 GHz, giving a sideband separation of 7.88 GHz. In order to cover the 330−360 GHz range as efficiently as possible, 35 pairs of unshifted/shifted spectra were taken. In each case a 'main' band was specified for operational convenience; in 25 cases this was the lower sideband, and in 10 cases the upper sideband.

Two Gunn oscillators were required in order to tune over the full 330−360 GHz range. For this and other operational reasons the frequency plan in main and image bands was quite complex and a small degree of overlap in coverage occurred, as shown in Fig. 3. From lines observed in both sidebands, the upper/lower sideband gain ratio was found to be close to unity. We have therefore assumed the sideband gains to be equal throughout these observations.

2.2. *Data reduction and presentation*

All 70 spectra taken are shown in Fig. 4, arranged in pairs. The upper panel shows the spectrum obtained at the centre frequency (given in the top right corner) and the lower panel shows the spectrum for a local oscillator shift of +10 MHz so that lines can be ascribed to the correct sideband, either 'main' or 'image'. The frequency scales shown on the upper and lower panels correspond respectively to the main and image sidebands and therefore run in opposite directions. For clarity, those identified lines found to lie in the main band are indicated in the upper panel. Image band lines are similarly marked on the lower panel.

Where possible, spectra from both sessions have been averaged together. All spectra have been binned over 2 or 4 channels according to the noise level and baselines subtracted. For session 1 data, this was always a constant offset whereas for session 2 data, it was occasionally necessary to remove a sinusoidal baseline of period ~ 300 MHz, reducing the sensitivity of these data. The noise level is typically of order $\sigma \simeq 0.16$ K. The constant continuum arising from dust and free-free emission from the ultracompact HII region within the beam has been subtracted from all spectra in Fig. 4.

All spectral lines detected were modelled with the SPECX gaussian fitting procedure and averaged values for the observed frequency, peak $T_{\rm A}^{*}$ and linewidth were calculated for each line. These data are listed in order of increasing frequency in Table 1. The fourth column contains a code indicating in which session the observation was made (1 or 2) and in which band the line was found (main, m, or image, i). Multiple independent detections of the same line are included. Observed frequencies in Table 1 have been corrected for two effects: a constant frequency offset in the AOSC and an error arising from the Doppler correction in the image sideband. The design of AOSC gave a constant offset of 2.9 MHz between the spectrometer centre channel and a spectral line in the middle of the IF passband which has been allowed for in subsequent reduction. Doppler correction of the local oscillator frequency to allow for the assumed +58 km s^{-1} velocity of the source relative to the LSR is only strictly correct at the centre frequency of the main band and is in error in the image band by ±1.5 MHz if the main band is the upper or lower sideband respectively. This frequency correction has been applied to observed frequencies in Table 1 and the frequency scales shown in Fig. 4.

2.3. *Line identification*

The frequencies of detected lines were compared with several lists of theoretical and laboratory-measured frequencies and with lines observed in other sources. These compilations included Lovas (1992), the Poynter and Pickett database (1985) and specific lists for the molecules methanol, CH_3OH (Anderson et al. 1993 and references therein), methyl formate, $HCOOCH_3$ (Plummer et al. 1987 and references therein), dimethyl ether, $(CH_3)_2O$ (E.Herbst, private communication) and ethanol, C_2H_5OH (Pearson et al. 1995). Observational lists included an informal catalogue compiled at the Nobeyama Radio Observatory and the list of Jewell et al. (1989) of lines detected in Orion-KL.

For each identified line, Table 1 lists the molecular species, the transition and rest frequency. Where there is more than one likely identification, all possibilities are listed, with the most plausible one indicated with an asterisk. For some molecules, most notably methyl formate, two or more transitions with the same lower-level energy lie within a few MHz. In these cases, only one transition is listed although its blended nature is marked in Table 1. The total number of detections listed is 447 lines, of which 109 are multiple detections, giving 338 independent spectral lines. The density of spectral lines detected in

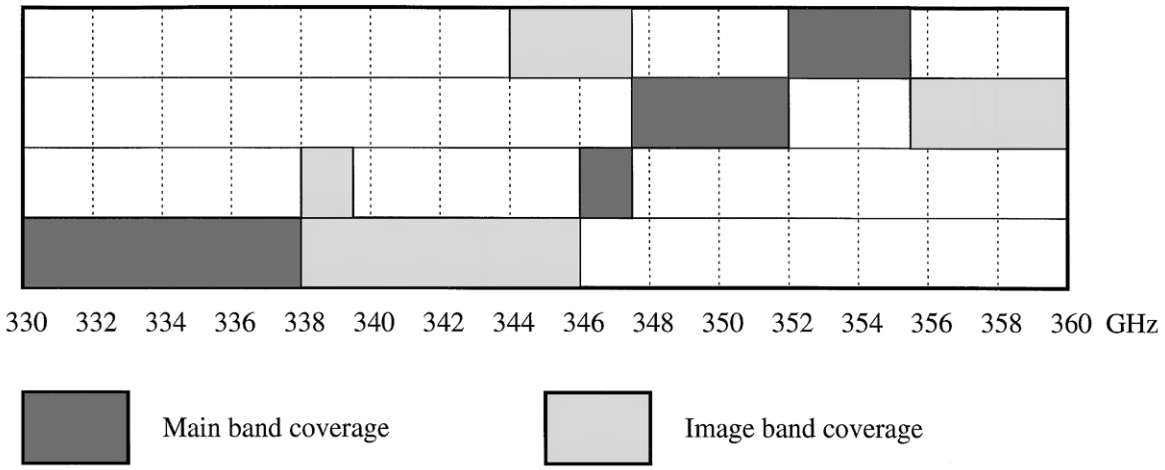

Fig. 3. Frequency plan showing ranges covered by main (dark) and image (light) sidebands for the 1992 March/April observing run. The centre frequencies of the two sidebands are separated by 7.88 GHz

G 34.3+0.15 is therefore 11.4 lines GHz^{-1} to a detection limit in $T_{\rm A}^*$ of about 0.5 K. This figure is similar to the detection frequency in Orion-KL of 5.4 lines GHz^{-1} (Jewell et al. 1989) and 8 lines GHz^{-1} (Avery et al. 1992) to a detection limit in $T_{\rm A}^*$ of 1 K over the same frequency range as for our survey and 9 lines GHz^{-1} over the range 257−273 GHz to a level of 0.8 K in $T_{\rm A}^*$ (Greaves & White 1991).

A few absorption features are seen in Fig. 4 which may arise either from molecular clouds along the line of sight to the background continuum source or from emission in the offset reference position. The absorption features associated with the J=3−2 ^{12}CO and ^{13}CO emission lines are almost certainly due to foreground material. The feature at 346.84 GHz is most probably an artefact of noise since it does not appear in the shifted spectrum.

Spectral lines have been identified with 35 distinct chemical species (some 40% of all presently known species in the ISM) plus 19 isotopomers, with possible detections of 6 further species. 70 lines remain unidentified: several of these lines were also detected in OMC1 (Jewell et al. 1989). As many as 14 lines are due to ethanol, making this the most comprehensive detection yet of this species in the interstellar medium (Millar et al. 1995).

The distribution of frequency difference between the observed and rest frequencies for each identified line was found to be Gaussian with a mean and standard deviation of 0.9±2.0 MHz, corresponding to a velocity difference of −0.8±1.8 km s^{-1}. Separate histograms for lines observed in both main and image bands in the two observing sessions are essentially identical, showing that there are no systematic errors in frequency measurement. The non-zero mean indicates that +57.2 km s^{-1} would have been a more appropriate choice of mean velocity relative to the LSR than the value of +58 km s^{-1} used. All the observed frequencies listed in Table 1 have therefore been corrected to this velocity. Figure 5 shows a histogram of the resulting frequency difference between observed and rest frequency for all identified lines. The observed dispersion of ±2.0 MHz arises from a combination of random measurement errors, self-absorption effects shifting the peak of some line profiles and an unknown spread in intrinsic velocity of different molecular species or between different excitation levels for a given species within the molecular cloud. The overall combination of these various effects must be relatively small (≤1.8 km s^{-1}) and detection of velocity change with energy level or between species will be difficult to observe in the presence of random errors in frequency measurement due to noise, particularly for the weaker lines. There is good evidence that this molecular cloud is in a state of collapse (Little et al. 1994), so some differentiation between species or energy level by velocity may nevertheless be expected and will be discussed in Paper II.

3. Data analysis

3.1. *Determination of column density: rotation diagrams*

Identified lines can be analysed using the rotation diagram technique (e.g. Turner 1991) which assumes optically thin emission from molecules in LTE. The total molecular column density can be obtained from

$$N_{\rm mol} = \frac{3k}{8\pi^3} \frac{\int T_R {\rm d}v}{\nu S \mu^2 g_I g_K} Q(T_{\rm rot}) \exp\left(\frac{E_{\rm u}}{kT_{\rm rot}}\right) \qquad (1)$$

Equation (1) can be rearranged to give

$$\log_{10}(L) = \log_{10}\left(\frac{N_{\rm mol}}{Q(T_{\rm rot})}\right) - \frac{E_{\rm u}}{k}\frac{\log_{10} e}{T_{\rm rot}} \qquad (2)$$

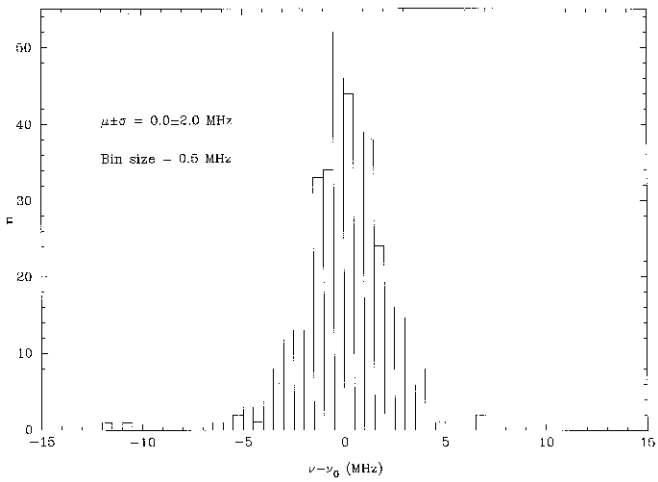

Fig. 5. Distribution of difference between the observed and rest frequencies for every identified spectral line in the survey. The dispersion is due to a combination of random errors in frequency measurement, significant optical depths leading to line asymmetries and spread in intrinsic velocity of emitting regions in different molecular species

where $L = \left(3k \int T_R \mathrm{d}v / 8\pi^3 \nu S \mu^2 g_K g_I\right)$, $\int T_R \mathrm{d}v$ is the integrated intensity, ν is the transition frequency, S is the line strength, μ is the permanent electric dipole moment and g_K and g_I are degeneracies. This is a straight line with a gradient of $(-\log_{10} e/T_{\rm rot})$ and a y-intercept of $\log_{10}(N_{\rm mol}/Q(T_{\rm rot}))$. These parameters were determined by using a linear regression routine to fit a straight line to the data. The uncertainty in $\int T_R \mathrm{d}v$ gives rise to an uncertainty in $\log_{10}(L)$, which has been plotted as 1-σ error bars on the rotation diagrams (Fig. 6). The quantity $W = \int T_R \mathrm{d}v$ was calculated from $\int T_R \mathrm{d}v \simeq 1.06 T_A^* \Delta v / \eta_{\rm fss}$, where it is assumed that the line is gaussian and the source-beam coupling factor, $\eta_{\rm c}$, is unity. Errors in fitting a straight line to the data are reflected in the corresponding errors in $T_{\rm rot}$ and $N_{\rm mol}$ given in Table 2.

The form of the partition function, $Q(T_{\rm rot})$, varies between molecular types. Assuming that the 'high-temperature' approximations are valid for all types of molecule, (i.e. $kT/h \gg B$, or whichever rotational constant is larger), the expressions for $Q(T_{\rm rot})$ given by Turner (1991) have been employed. Herzberg (1945) pp. 505-506 discusses the validity of these approximations, and for most molecules the error in the partition function should not be significant for $T_{\rm rot} \gtrsim 25$ K. For highly asymmetric molecules such as HDO and SHD, the partition function was estimated by interpolation between values given at various temperatures by Poynter & Pickett (1985).

3.2. *Determination of column density: single detections*

For those molecules with only one or two detections, a lower limit to the total column density has been estimated. As before, LTE populations and low optical depth are assumed. The choice of rotation temperature in equation (1) has been determined by equating the derivative of the temperature dependent part of the equation to zero: i.e. $\frac{\rm d}{\rm dT}(Q(T)\exp(E_{\rm u}/kT)) = 0$, where $Q(T)$ takes on the appropriate form for each molecule. For a linear molecule, it may be shown that this rotation temperature is equal to $E_{\rm u}/k$. For symmetric or slightly asymmetric tops, $T_{\rm rot} = \frac{2}{3}E_{\rm u}/k$. Forming the second derivative shows that these turning points are minima, and thus strict lower limits to $N_{\rm mol}$ can be derived.

3.3. *Relative abundances*

For all those molecules with at least three identified transitions, rotation diagrams were plotted and are shown in Fig. 6. The straight-line fits are plotted on these figures and the rotation temperatures and molecular column densities are tabulated in Table 2, along with the corresponding 1-σ uncertainties derived formally from the fit. The lower limits estimated from the molecules with only single or double detections are tabulated in Table 3. No errors are presented in this table as the values are all lower limits. The identification of a few species on the basis of one or two lines is very insecure. For example HCOOD and $\rm H^{13}COOH$, are non-linear rotors and should have several transitions in this frequency range.

The rotation temperature and molecular column density given in Table 2 for ethanol differ slightly from the previously published values (Millar et al. 1995) since the measured $T_{\rm A}^*$ had there been corrected for coupling between the source and the telescope beam. Furthermore, the coupling efficiency had been assumed to vary slightly with frequency across the 30 GHz range of the survey. Since we have no information on any size variation of the molecular cloud between species, no attempt has been made here to correct for the effect of beam coupling to the source.

4. Summary and Conclusions

We have carried out a submillimetre wave spectral survey of the hot molecular core in G 34.3+0.15, covering the complete frequency range from 330 to 360 GHz. A total of 338 spectral features were detected down to limiting values in T_A^* of 0.3 K. Of these, 268 have been identified with 35 distinct molecular species, plus 19 isotopically substituted variants. 70 lines remain unidentified: several of these are also seen in the Orion molecular cloud.

Rotation temperature and chemical abundance have been determined for 50 species and isotopomers. For 12 species these are firm values from rotation diagram analysis. Column density estimates for the remainder are

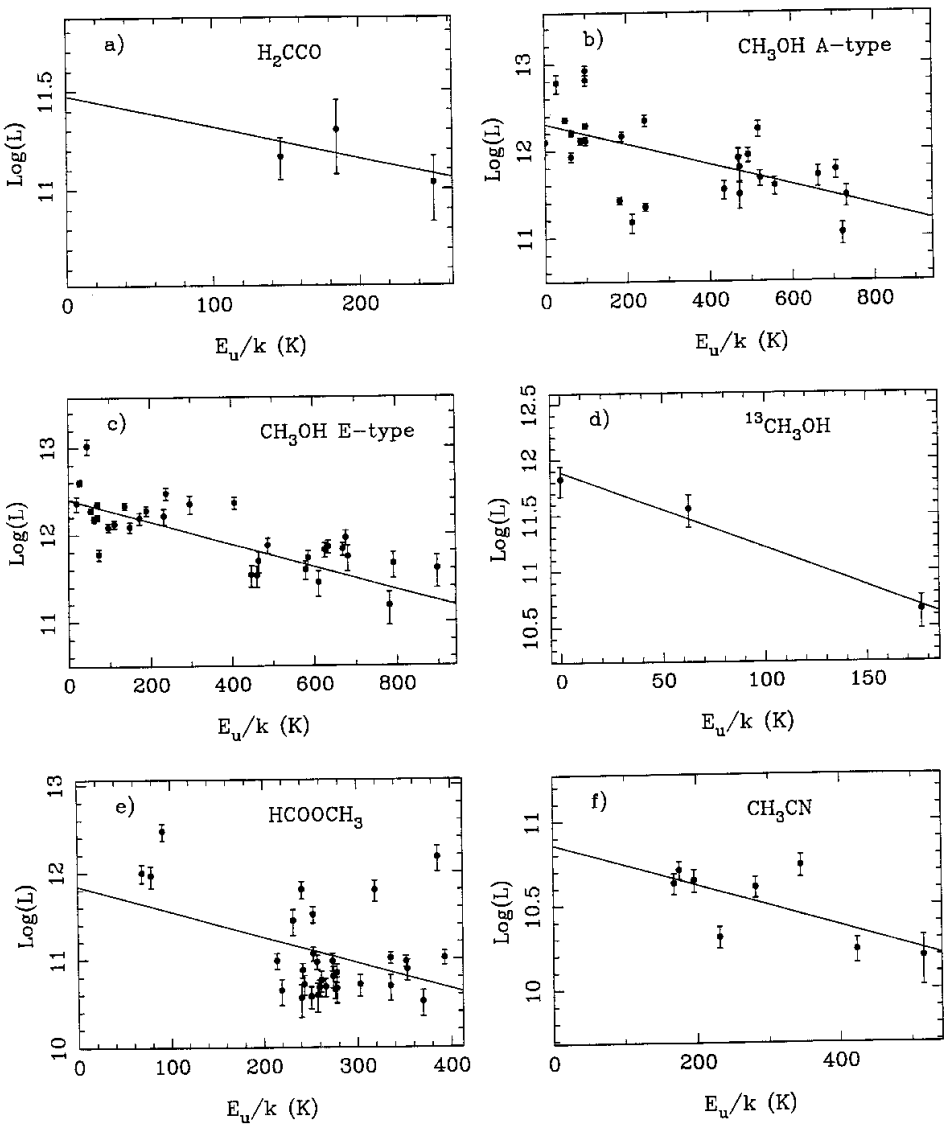

Fig. 6. Rotation diagrams for molecules with at least three detected transitions. On each figure, points which have been included in the straight line fit are denoted by filled circles. The error bars represent ± 1-σ. Where a two-temperature fit has been attempted, the lower temperature points are marked by filled circles and the higher temperature points marked by filled triangles, although the fit for the latter has not always been shown. The *A*- and *E*-type methanol species are presented in separate diagrams

lower limits where only one or two lines have been detected.

The species detected reflect the diverse physical conditions within the G 34.3 molecular cloud. Complex molecules and vibrationally excited HCN, indicative of hot molecular cores, have been detected as have the molecular ion HCS^+ and highly unsaturated and radical species such as NO, SO and H_2CCO, which probably arise in the outer envelope of the cloud. Detailed chemical models of this source, taking into account the three-component structure of the molecular clouds, are being constructed and a discussion of the significance of these data for understanding the chemical evolution of hot molecular cores will be given in a subsequent paper (Paper II).

Despite the wealth of molecular lines detected in this survey, we have been unable to obtain abundance estimates for many of the diatomic and triatomic species as we have often detected only one transition. Observations at other frequencies, and of isotopomers, will be needed to derive optical depth, rotation temperature and abundance in order to further constrain models of this source.

Acknowledgements. We are grateful to the staff of the JCMT for assistance in making these observations. RJH

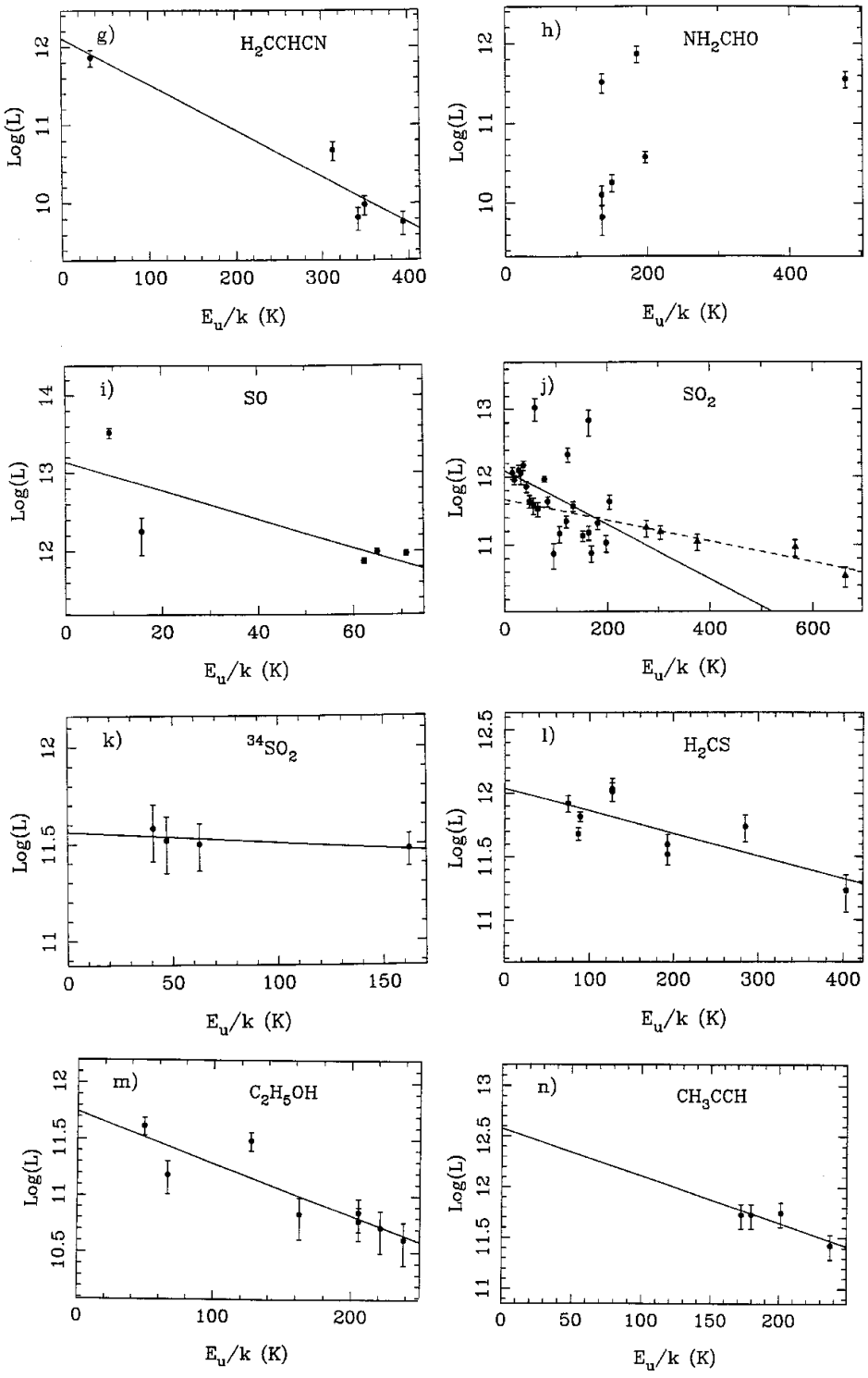

Fig. 6. continued

acknowledges support by a research grant from the EC (ERBSC1*CT005066). AGG is supported by a PPARC Postdoctoral Research Fellowship. We would like to thank the referee, Dr. M.Guélin, for his suggestions which have led to an improved version of this paper. The JCMT is operated by the Royal Observatories on behalf of the Particle Physics and Astronomy Research Council of the UK, the Netherlands Organisation for Scientific Research and the National research Council of Canada.

References

Anderson T., Herbst E., De Lucia F.C., 1993, J. Mol. Spectrosc. 159, 410
Avery L.W., Amano T., Bell M.B., et al., 1992, ApJ 83, 363
Blake G.A., Sutton E.C., Masson C.R., Phillips T.G., 1986, ApJS 60, 357
Cummins S.A., Linke R.A., Thaddeus P., 1986, ApJS 60, 819
Gaume R.A., Fey A.L., Claussen M.J., 1994, ApJ 432, 648
Greaves J.S., White G.J., 1991 A&AS 91, 237
Heaton B.D., Little L.T., Yamashita T., Monteiro T.S., Cunningham C.T., Davies S.R., 1993, A&A 278, 238
Heaton B.D., Little L.T., Bishop I.S., 1989, A&A 213, 148
Herzberg G., 1945, Molecular spectra and molecular structure Vol.2: Infrared and Raman spectra of polyatomic molecules, London: Van Nostrand Reinhold
Jewell P.R., Hollis J.M., Lovas F.J., Snyder L.E., 1989, ApJS 70, 833
Johansson L.E.B., Andersson C., Ellder J., et al., 1984, A&A 130, 227
Kutner M.L., Ulich B.L., 1981, ApJ 250, 341
Little L.T., Gibb A.G., Heaton B.D., Claude S.M.X., Ellison B.N., 1994, MNRAS 271, 649
Lovas F.J., 1992, J. Phys. Chem. Ref. Data 21, 181
Millar T.J., Macdonald G.H., Habing R.J., 1995 MNRAS 273, 25
Pearson J.C., Sastry K.V.L.N., Winnewisser M., Herbst E., De Lucia F.C., 1995, J. Phys. Chem. Ref. Data (submitted)
Plummer G.M., Herbst E., De Lucia F.C., 1987, ApJ 318, 873
Poynter R.L., Pickett H.M., 1985, Applied Opt. 24, 2335
Strong-Jones F.S., Heaton B.D., Little L.T., 1991, A&A 251, 263
Sutton E.C., Blake G.A., Masson C.R., Phillips T.G., 1985, ApJS 53, 341
Turner B.E., 1989, ApJS 70, 539
Turner B.E., 1991, ApJS 76, 617
Van Buren D., MacLow M.-M., Wood D.O.S., Churchwell E., 1990, ApJ 353, 570
Walmsley C.M., 1992, in Chemistry and Spectroscopy of Interstellar Molecules. In: Bohme D.K., Herbst E., Kaifu N., Saito S. (eds.). Tokyo: Tokyo University Press, p. 267
Wood D.O.S., Churchwell E., 1989, ApJS 69, 831

Table 1. Parameters of spectral lines detected, giving observed frequency, ν(obs), line brightness T_A^* and line width. All entries represent independent observations.The code in column 4 indicates whether the line was detected in the first (1) or second (2) observing session, in the main (m) or image (i) band. During run 2, some overlapping coverage occurred, with the same line appearing in upper and lower sideband on different frequency settings. The remaining columns show the species and transition identified with the line, and the corresponding rest frequency. If the identification is ambiguous, the various alternatives are given, with the favoured identification shown with an asterisk. Question marks denote uncertain detections and blended lines are marked by 'b'. All the $HCOOCH_3$ lines are of the $A-$species. Some of the $HCOOCH_3$, C_2H_5CN and H_2CCHCN identifications are blends of two or more transitions of equivalent energy, as is the NS line, all marked by 'b'. The NH_2CHO lines are blends of several hyperfine components

ν(obs) (GHz)	T_A^* (K)	Width (MHz)	code	Species	Transition	ν(rest) (GHz)	Notes
330.0359	0.7	6.6	2m	U			
330.1917	0.7	5.9	2m	$H_2{}^{13}CS$	10(3,8)–9(3,7)	330.1958	
330.3532	0.8	10.6	2m	CH_3OH	20(3)–19(4) $A-$	330.3554	
330.3738	0.7	9.4	2m	H_2CCHCN	11(3,8)–10(2,9)	330.3719	
330.4074	0.7	6.0	2m	$(CH_3)_2O$	15(1,14)–16(2,15)	330.4076	
330.4089	0.7	13.2	1m	$(CH_3)_2O$	15(1,14)–16(2,15)	330.4076	
330.4607	0.7	8.7	2m	NH_2CHO	19(1,18)–18(2,17)	330.4596	
330.5891	(10)	(20)	1m	^{13}CO	3–2	330.5879	self-absorbed
330.5891	(10)	(20)	2m	^{13}CO	3–2	330.5879	self-absorbed
331.0404	1.2	14.7	2m	CH_3CN	18(2)–17(2)	331.0465	
331.0721	1.3	10.6	2m	CH_3CN	18(1)–17(1)	331.0652	b
				CH_3CN	18(0)–17(0)	331.0719	
331.2215	0.8	11.0	2m	CH_3OH	16(–1)–15(–2) E	331.2216	
331.4671	0.5	6.2	2m	$HCOOCH_3$	28(3,25)–27(3,24)	331.4697	
332.0915	0.7	13.5	2m	SO_2	21(2,20)–21(1,21)	332.0914	b
				CH_3OH	21(5)–22(4) E	332.0874	
332.5045	0.8	14.5	1m	SO_2	4(3,1)–3(2,2)	332.5053	
332.5315	0.6	10.8	1m	H_2CCHCN	35(6,30)–34(6,29)	332.5325	b
332.5735	0.9	14.1	1m	$HCOOCH_3$	30(1,29)–29(1,28)	332.5764	b
332.5737	0.6	15.5	2m	$HCOOCH_3$	30(1,29)–29(1,28)	332.5764	b
333.1113	0.5	9.9	1m	$^{13}CH_3OH$	7(1)–6(1) $A-$	333.1148	
333.1167	0.5	13.1	2m	$^{13}CH_3OH$	7(1)–6(1) $A-$	333.1148	
333.1185	0.4	10.9	1m	$H^{13}COOH$	13(3,11)–13(2,12)	333.1208	
333.1621	0.5	7.3	2m	U			
333.2781	0.3	8.3	1m	SHD	2(0,2)–1(1,1)	333.2786	
333.4195	0.6	7.3	2m	$HCOOCH_3$	27(12,15)–26(12,14)	333.4190	b
333.4381	0.6	10.5	2m	U			
333.4492	0.9	7.3	2m	$HCOOCH_3$	31(0,31)–30(0,30)	333.4496	b
333.4504	0.5	11.8	1m	$HCOOCH_3$	31(0,31)–30(0,30)	333.4496	b
333.9032	0.6	7.3	2m	^{34}SO	7(8)–6(7)	333.9010	
334.4275	0.7	8.4	2m	CH_3OH	3(0)–2(1) E	334.4266	
334.4569	0.5	8.4	2m	U			
334.6751	0.9	10.2	2m	SO_2	8(2,6)–7(1,7)	334.6733	
334.7096	0.6	7.7	2m	NH_2CHO	17(0,17)–16(1,16)	334.7100	
334.8733	0.6	9.8	2m	$HCOOCH_3$	27(10,17)–26(10,16)	334.8727	
334.8930	0.6	8.0	2m	U			
335.1352	0.7	8.0	2m	CH_3OH	2(2)–3(1) $A-$	335.1335	
335.3971	0.6	6.2	2m	HDO	3(3,1)–4(2,2)	335.3954	
335.5604	0.5	7.3	2m	$^{13}CH_3OH$	12(1)–12(0) $A+$	335.5660	
335.5607	0.5	5.2	1m	$^{13}CH_3OH$	12(1)–12(0) $A+$	335.5660	
335.5831	1.2	7.5	1m	CH_3OH	7(1)–6(1) $A+$	335.5820	
335.5844	2.0	10.5	2m	CH_3OH	7(1)–6(1) $A+$	335.5820	
335.9649	0.6	7.3	2m	U			
336.0278	0.6	9.1	2m	$HCOOCH_3$	27(9,19)–26(9,18)	336.0281	
336.3511	0.6	12.3	1m	NH_2CHO	29(4,25)–29(3,26)	336.3514	
336.3541	0.9	9.5	2m	NH_2CHO	29(4,25)–29(3,26)	336.3514	
336.3726	0.9	10.2	2m	$HCOOCH_3$	26(5,21)–25(5,20)	336.3739	
336.3749	0.7	14.2	1m	$HCOOCH_3$	26(5,21)–25(5,20)	336.3739	
336.4387	0.5	9.1	2m	CH_3OH	14(7)–15(6) $A+$, $A-$	336.4383	
336.5218	0.7	9.7	1m	HC_3N	37–36	336.5212	
336.8654	2.1	8.7	2m	CH_3OH	12(1)–12(0) $A+$, $A-$	336.8651	

Table 1. continued

ν(obs) (GHz)	T_A^* (K)	Width (MHz)	code	Species	Transition	ν(rest) (GHz)	Notes
336.8872	0.7	9.8	2m	U			
336.9184	0.5	8.7	2m	$HCOOCH_3$	26(6,20)–25(6,19)	336.9181	
337.0604	2.6	8.4	2m	$C^{17}O$	3–2	337.0611	
337.1366	0.8	8.0	2m	CH_3OH	4(2)–3(3) E	337.1359	
337.1370	0.9	10.8	1m	CH_3OH	4(2)–3(3) E	337.1359	
337.1498	0.4	4.6	1m	U			
337.1770	0.5	10.2	1m	CH_3OH	7(–4)–6(–4) E vt2	337.1751	
337.1902	0.4	6.3	1m	CH_3OH	7(0)–6(0) E vt2	337.1865	
337.1993	0.5	8.9	1m	CH_3OH	7(–5)–6(–5) E vt2	337.1985	
337.2497	0.7	11.3	2m	CH_3OH	7(3)–6(3) $A+$,$A-$ vt2	337.2522	
337.2743	0.6	7.3	2m	CH_3OH	7(4)–6(4) $A+$,$A-$ vt2	337.2735	
337.2838	0.9	9.5	1m	CH_3OH	7(0)–6(0) $A+$ vt2	337.2843	
337.2855	0.6	8.0	2m	CH_3OH	7(0)–6(0) $A+$ vt2	337.2843	
337.2986	1.0	9.1	2m	CH_3OH	7(3)–6(3) E vt2	337.2958	
337.2998	1.0	10.8	1m	CH_3OH	7(2)–6(2) E vt2	337.3026	
337.3106	0.7	8.0	1m	CH_3OH	7(–1)–6(–1) E vt2	337.3123	
337.3139	0.7	10.2	2m	CH_3OH	7(–1)–6(–1) E vt2	337.3123	
337.3283	0.4	6.3	1m	C_2H_5OH	20(7,14)–20(6,15)	337.3250	
337.3479	0.4	10.2	1m	C_2H_5CN	38(3,36)–37(3,35)	337.3470	in OMC1 (U337.353)
337.3943	2.4	6.4	2m	$C^{34}S$	7–6	337.3966	
337.3948	2.5	8.6	1m	$C^{34}S$	7–6	337.3966	
337.4242	0.6	6.9	2m	H_2NCN vt1	17(1,17)–16(1,16)	337.4278	
337.4242	0.4	7.9	1m	H_2NCN vt1	17(1,17)–16(1,16)	337.4278	
337.4616	0.6	6.0	1m	$H_2C^{34}S$	10(4,6)–9(4,5)	337.4619	b
337.4645	0.8	9.5	2m	CH_3OH	7(6)–6(6) $A+$ vt1	337.4637	b
337.4903	0.8	11.6	2m	CH_3OH	7(6)–6(6) $A-$ vt1	337.4905	
337.4909	0.5	8.1	1m	CH_3OH	7(6)–6(6) $A-$ vt1	337.4905	
337.5186	0.6	11.0	1m	CH_3OH	7(3)–6(3) E vt1	337.5191	
337.5470	0.6	10.9	1m	CH_3OH	7(5)–6(5) $A+$ vt1	337.5461	
337.5832	0.9	8.2	1i	^{34}SO	8(8)–7(7)	337.5802	b
				CH_3OH	7(4)–6(4) E vt1	337.5817	
337.6719	0.6	8.7	2m	CH_3OH	7(2)–6(2) E vt1	337.6712	
337.6864	0.6	8.4	2m	CH_3OH	7(5)–6(5) E vt1	337.6853	
337.7089	0.6	9.1	2m	CH_3OH	7(–1)–6(–1) E vt1	337.7075	
337.7252	0.4	7.5	2m	C_2H_5OH	19(7,12)–19(6,13)	337.7280	
337.7328	0.5	6.9	2m	U			
337.7495	0.5	10.2	2m	CH_3OH	7(0)–6(0) $A+$ vt1	337.7488	
337.8291	0.5	8.4	2m	U			
337.8444	0.4	6.9	2m	U			
337.8789	0.6	8.0	2m	CH_3OH	7(1)–6(1) A vt2	337.8775	
337.8937	0.4	8.0	2m	SO_2 v2=1	21(2,20)–21(1,21)	337.8922	
337.9696	0.8	7.3	2m	U			in OMC1 (U337.973)
337.9698	0.9	7.1	2i	U			
338.0814	2.2	7.6	2i	H_2CS	10(1,10)–9(1,9)	338.0810	
338.0814	1.4	9.1	2i	H_2CS	10(1,10)–9(1,9)	338.0810	
338.0978	0.5	7.7	2i	C_2H_5OH	18(7,11)–18(6,12)	338.0990	
338.1069	0.5	6.4	2i	C_2H_5OH	18(7,12)–18(6,13)	338.1100	
338.1232	3.3	9.0	2i	CH_3OH	7(0)–6(0) E	338.1245	
338.1232	2.3	9.1	2i	CH_3OH	7(0)–6(0) E	338.1245	
338.3057	0.8	11.3	1i	SO_2	18(4,14)–18(3,15)	338.3060	
338.3067	0.8	9.7	2i	SO_2	18(4,14)–18(3,15)	338.3060	
338.3448	3.6	10.7	1i	CH_3OH	7(–1)–6(–1) E	338.3446	
338.3448	3.8	9.1	2i	CH_3OH	7(–1)–6(–1) E	338.3446	
338.3438	2.4	9.2	2i	CH_3OH	7(–1)–6(–1) E	338.3446	
338.3557	0.6	6.2	2i	$HCOOCH_3$	27(8,19)–26(8,18)	338.3558	
338.3929	0.8	8.9	2i	CH_3OH	7(6)–6(6) E	338.4046	
338.4084	4.0	9.5	1i	CH_3OH	7(0)–6(0) $A+$	338.4087	
338.4086	4.4	11.4	2i	CH_3OH	7(0)–6(0) $A+$	338.4087	

Table 1. continued

ν(obs) (GHz)	T_A^* (K)	Width (MHz)	code	Species	Transition	ν(rest) (GHz)	Notes
338.4074	3.3	8.7	2i	CH_3OH	7(0)–6(0) $A+$	338.4087	
338.4307	1.8	11.1	2i	CH_3OH	7(–6)–6(–6) E	338.4310	
338.4291	0.8	8.0	2i	CH_3OH	7(–6)–6(–6) E	338.4310	
338.4325	1.1	15.9	1i	CH_3OH	7(–6)–6(–6) E	338.4310	
338.4425	1.0	7.3	2i	CH_3OH	7(6)–6(6) $A+$,$A-$	338.4424	
338.4429	1.1	7.5	1i	CH_3OH	7(6)–6(6) $A+$,$A-$	338.4424	
338.4412	1.6	9.5	2i	CH_3OH	7(6)–6(6) $A+$,$A-$	338.4424	
338.4579	1.1	11.5	1i	CH_3OH	7(–5)–6(–5) E	338.4565	
338.4565	0.8	9.8	2i	CH_3OH	7(–5)–6(–5) E	338.4565	
338.4552	1.8	11.0	2i	CH_3OH	7(–5)–6(–5) E	338.4565	
338.4737	1.1	8.7	2i	CH_3OH	7(5)–6(5) E	338.4753	
338.4734	1.8	13.5	2i	CH_3OH	7(5)–6(5) E	338.4753	
338.4863	1.2	6.9	2i	CH_3OH	7(5)–6(5) $A+$,$A-$	338.4863	
338.4879	1.8	9.4	2i	CH_3OH	7(5)–6(5) $A+$,$A-$	338.4863	
338.5034	1.9	12.6	2i	CH_3OH	7(–4)–6(–4) E	338.5041	
338.5124	2.2	8.1	2i	CH_3OH	7(2)–6(2) $A-$	338.5128	
338.5131	1.9	14.9	2i	CH_3OH	7(4)–6(4) $A-$,$A+$	338.5128	
338.5294	1.8	10.9	1i	CH_3OH	7(4)–6(4) E	338.5302	
338.5288	1.7	9.9	2i	CH_3OH	7(4)–6(4) E	338.5302	
338.5299	0.9	8.7	2i	CH_3OH	7(4)–6(4) E	338.5302	
338.5421	3.0	9.6	1i	CH_3OH	7(3)–6(3) $A+$	338.5408	
338.5406	2.7	9.0	2i	CH_3OH	7(3)–6(3) $A+$	338.5408	
338.5422	1.8	9.8	2i	CH_3OH	7(3)–6(3) $A-$	338.5432	
338.5598	1.7	11.6	1i	CH_3OH	7(–3)–6(–3) E	338.5599	
338.5587	1.7	9.7	2i	CH_3OH	7(–3)–6(–3) E	338.5599	
338.5825	2.0	9.2	1i	CH_3OH	7(3)–6(3) E	338.5832	
338.5824	1.8	8.4	2i	CH_3OH	7(3)–6(3) E	338.5832	
338.5805	1.5	10.6	2i	CH_3OH	7(3)–6(3) E	338.5832	
338.6143	3.0	10.6	1i	CH_3OH	7(1)–6(1) E	338.6150	
338.6141	2.4	10.0	2i	CH_3OH	7(1)–6(1) E	338.6150	
338.6143	2.7	8.7	2i	CH_3OH	7(1)–6(1) E	338.6150	
338.6395	2.6	10.1	1i	CH_3OH	7(2)–6(2) $A+$	338.6399	
338.6386	2.0	10.0	2i	CH_3OH	7(2)–6(2) $A+$	338.6399	
338.6404	2.1	7.3	2i	CH_3OH	7(2)–6(2) $A+$	338.6399	
338.7088	0.6	7.9	1i	U			
338.7197	3.0	9.1	2i	CH_3OH	7(2)–6(2) E	338.7216	
338.7204	3.7	10.6	2i	CH_3OH	7(2)–6(2) E	338.7216	
338.7224	3.4	10.5	1i	CH_3OH	7(2)–6(2) E	338.7216	
338.7470	0.7	5.8	2i	U			
338.7598	1.3	8.7	2i	U			
338.7714	0.8	6.9	2i	U			
338.8434	0.8	3.0	2i	U			
338.8879	0.4	7.2	2i	C_2H_5OH	15(7,8)–15(6,9)	338.8860	b
				C_2H_5OH	15(7,9)–15(6,10)	338.8870	
339.3105	0.9	10.2	2i	C_2H_5OH	12(7,5)–12(6,6)	339.3130	
339.3100	1.1	9.5	2i	C_2H_5OH	12(7,6)–12(6,7)	339.3130	
339.3385	1.2	14.4	2i	SO	3(3)–3(2)	339.3415	
339.3392	1.1	6.9	2i	SO	3(3)–3(2)	339.3415	
339.4607	0.5	6.6	2i	CN	3–2 2.5 1.5–2.5 2.5	339.4600	
339.4623	0.5	8.5	2i	CN	3–2 2.5 2.5–2.5 1.5	339.4627	
339.4915	0.7	9.1	2i	$(CH_3)_2O$	18(2,17)–19(1,18)	339.4915	b
				CN	3–2 2.5 2.5–1..5 1.5	339.4933	
339.8563	0.6	8.0	2i	^{34}SO	9(8)–8(7)	339.8573	
340.0380	2.1	6.7	2i	CN	3–2 2.5 2.5–1.5 1.5	340.0355	
340.0543	1.4	9.9	2i	$C^{33}S$	7–6	340.0527	
340.1409	1.3	10.9	2i	NH_2CHO	16(5,11)–15(5,10)	340.1376	b
				CH_3OH	2(2)–3(1) $A+$, $A-$	340.1412	
340.1889	0.9	13.3	2i	C_2H_5OH	6(5,1)–5(4,2)	340.1890	b
				C_2H_5OH	6(5,2)–5(4,1)	340.1890	
340.2510	3.6	5.4	1i	CN	3–2 3.5 3.5–2.5 2.5	340.2478	

Table 1. continued

ν(obs) (GHz)	T_A^* (K)	Width (MHz)	code	Species	Transition	ν(rest) (GHz)	Notes
340.2514	3.7	4.5	2i	CN	3–2 3.5 4.5–2.5 3.5	340.2479	
340.2647	0.9	15.5	1i	CN	3–2 3.5 3.5–2.5 3.5	340.2630	
340.2656	0.7	21.8	2i	CN	3–2 3.5 2.5–2.5 2.5	340.2618	
340.3166	0.6	9.0	1i	SO_2	28(2,26)–28(1,27)	340.3165	
340.3948	0.9	10.5	1i	CH_3OH	16(6)–17(5) $A+$,$A-$	340.3942	
340.4369	0.4	6.8	1i	U			
340.4484	1.5	10.7	1i	OCS	28–27	340.4493	
340.4504	1.1	10.6	2i	OCS	28–27	340.4493	
340.6113	0.7	16.5	1i	$(CH_3)_2O$	9(2,8)–10(3,7)	340.6150	
340.6137	0.7	11.6	2i	$(CH_3)_2O$	9(2,8)–10(3,7)	340.6160	
340.6293	0.5	4.0	1i	$HC^{18}O^+$	4–3	340.6307	
340.6839	0.8	10.5	2i	CH_3OH	11(1)–10(0) E vt1	340.6842	
340.6841	0.9	19.2	1i	CH_3OH	11(1)–10(0) E vt1	340.6842	b?
340.7131	3.0	9.7	1i	SO	7(8)–6(7)	340.7143	
340.7148	2.2	9.8	2i	SO	7(8)–6(7)	340.7143	
341.1323	0.7	8.9	2i	U			
341.1309	0.7	9.8	1i	U			
341.1733	0.5	7.6	2i	U			
341.2361	0.4	11.9	1i	U			
341.2428	0.5	6.9	2i	HCO	11(0,11)–10(1,10)	341.2426	
341.3498	0.7	9.9	1i	HCS^+	8–7	341.3501	
341.4151	2.4	10.1	1i	CH_3OH	7(1)–6(1) $A-$	341.4155	
341.4166	3.4	8.7	2i	CH_3OH	7(1)–6(1) $A-$	341.4155	
341.4671	0.4	12.7	2i	U			
341.6755	0.5	7.3	2i	SO_2	36(5,31)–36(4,32)	341.6743	
341.6828	0.6	7.3	2i	CH_3CCH	20(3)–19(3)	341.6837	
341.7162	0.6	8.0	2i	CH_3CCH	20(2)–19(2)	341.7154	
341.7361	0.7	12.4	2i	CH_3CCH	20(1)–19(1)	341.7346	b
				CH_3CCH	20(0)–19(0)	341.7411	
341.9199	0.5	8.4	2i	H_2CCHCN	36(7,29)–35(7,28)	341.9235	
342.2906	0.4	8.4	2i	U			
342.3135	0.5	9.8	2i	H_2CCHCN	36(5,32)–35(5,31)	342.3169	
342.3527	0.8	6.5	2i	$HCOOCH_3$	30(2,28)–29(3,27)	342.3504	
342.3618	0.9	15.4	2i	$HCOOCH_3$	30(3,28)–29(3,27)	342.3597	b
				$HCOOCH_3$	30(2,28)–29(2,27)	342.3665	
342.6087	1.0	8.2	2i	$(CH_3)_2O$	18(1,18)–19(0,19)	342.6080	
342.6936	0.6	9.1	2i	$HCOOCH_3$	27(13,15)–27(12,16)	342.6899	b
342.7292	2.6	10.2	2i	CH_3OH	13(1)–13(0) $A+$,$A-$	342.7298	
342.7289	0.4	12.3	1i	CH_3OH	13(1)–13(0) $A+$,$A-$	342.7298	
342.7626	0.6	12.0	2i	SO_2	34(3,31)–34(2,32)	342.7619	
342.8859	9.6	5.2	2i	CS	7–6	342.8829	
342.8856	4.5	6.0	1i	CS	7–6	342.8829	
342.8828	4.2	5.8	1m	CS	7–6	342.8829	
342.9458	1.2	7.3	2i	H_2CS	10(0,10)–9(0,9)	342.9443	
343.0859	0.7	8.0	2i	NH_2CHO	16(3,13)–15(3,12)	343.0831	
343.1497	0.6	16.0	1m	$HCOOCH_3$	17(5,12)–16(4,13)	343.1499	b
343.1506	1.0	8.0	2i	$HCOOCH_3$	17(5,12)–16(4,13)	343.1499	b
343.1519	0.9	13.0	1m	$HCOOCH_3$	31(1,30)–30(1,29)	343.1535	b
343.1978	0.4	5.7	1i	NH_2CHO	17(1,17)–16(1,16)	343.1970	
343.2035	0.5	8.1	1i	H_2CS	10(5,5)–9(5,4)	343.2011	b
343.3071	0.7	6.9	2i	H_2CS	10(4,7)–9(4,6)	343.3076	b
343.3136	0.5	10.6	1i	U			
343.3205	0.8	13.7	1i	H_2CS	10(2,9)–9(2,8)	343.3198	
343.3233	1.5	8.7	2i	$H_2{}^{13}CO$	5(1,5)–4(1,4)	343.3257	
343.3244	1.8	9.1	1i	$H_2{}^{13}CO$	5(1,5)–4(1,4)	343.3257	
343.3868	0.5	9.1	1m	H_2CCO	17(3,14)–16(3,13)	343.3883	
343.3880	0.4	9.6	1i	H_2CCO	17(3,14)–16(3,13)	343.3883	
343.4079	0.8	13.6	2i	H_2CS	10(3,8)–9(3,7)	343.4077	
343.4088	0.9	13.3	1i	H_2CS	10(3,8)–9(3,7)	343.4077	

Table 1. continued

ν(obs) (GHz)	T_A^* (K)	Width (MHz)	code	Species	Transition	ν(rest) (GHz)	Notes
343.4101	0.7	11.2	1m	H_2CS	10(3,7)–9(3,6)	343.4119	
343.4132	1.3	9.4	2i	H_2CS	10(3,7)–9(3,6)	343.4119	
343.4147	1.0	9.1	1m	H_2CS	10(3,7)–9(3,6)	343.4119	
343.4362	0.6	8.4	2i	U			
343.4460	0.4	10.1	1m	$HCOOCH_3$	28(4,24)–27(4,23)	343.4442	
343.6966	0.4	6.6	1m	H_2CCO	17(2,15)–16(2,14)	343.6939	
343.7546	0.9	8.0	2i	$HCOOCH_3$	27(7,20)–26(7,19)	343.7580	
343.7566	0.9	9.4	1m	$HCOOCH_3$	27(7,20)–26(7,19)	343.7580	
343.8107	1.0	10.5	1m	H_2CS	10(2,8)–9(2,7)	343.8109	
343.8620	0.4	8.8	1m	^{34}SO	2(3)–2(1)	343.8651	
343.9837	0.6	10.2	2i	$OC^{34}S$	29–28	343.9833	
343.9848	0.4	7.8	1m	$OC^{34}S$	29–28	343.9833	
344.0303	0.8	7.8	1m	$HCOOCH_3$	32(0,32)–31(0,31)	344.0298	b
344.1078	0.9	8.4	2i	CH_3OH	18(2)–17(3) E	344.1104	
344.1080	0.7	14.5	1m	CH_3OH	18(2)–17(3) E	344.1104	
344.1087	0.9	9.1	2i	CH_3OH	18(2)–17(3) E	344.1104	
344.1100	1.0	9.7	1m	CH_3OH	18(2)–17(3) E	344.1104	
344.2006	1.3	10.1	1i	$HC^{15}N$	4–3	344.2003	
344.1995	1.4	9.1	2i	$HC^{15}N$	4–3	344.2003	
344.2017	1.4	6.6	2i	$HC^{15}N$	4–3	344.2003	
344.2884	0.6	8.4	2i	U			
344.3097	2.2	11.0	1i	SO	8(8)–7(7)	344.3107	
344.3102	3.3	9.1	2i	SO	8(8)–7(7)	344.3107	
344.3103	3.1	9.4	2i	SO	8(8)–7(7)	344.3107	
344.3572	0.8	11.3	1i	$(CH_3)_2O$	18(0,18)–19(1,19)	344.3580	
344.3574	0.7	9.5	2i	$(CH_3)_2O$	18(0,18)–19(1,19)	344.3580	
344.3582	0.7	8.0	2i	$(CH_3)_2O$	18(0,18)–19(1,19)	344.3580	
344.4430	0.7	12.6	1i	CH_3OH	19(1)–18(2) $A+$	344.4447	
344.4436	0.8	8.8	2i	CH_3OH	19(1)–18(2) $A+$	344.4447	
344.4443	0.6	7.6	2i	CH_3OH	19(1)–18(2) $A+$	344.4447	
344.5141	0.6	17.7	1i	$HCOOCH_3$	28(16,13)–27(16,12)	344.5149	b
344.5149	0.9	9.1	2i	$HCOOCH_3$	28(16,13)–27(16,12)	344.5149	b
344.5173	0.6	7.3	2i	$(CH_3)_2O$	10(2,8)–11(2,9)	344.5186	
344.9166	0.8	11.3	2i	SiO v=1	8–7	344.9163	
345.0687	0.6	11.3	2i	$HCOOCH_3$	28(14,15)–27(14,14)	345.0685	b
345.1490	0.5	8.0	2i	SO_2	5(5,1)–6(4,2)	345.1491	
345.1486	0.4	8.9	1m	SO_2	5(5,1)–6(4,2)	345.1491	
345.1820	0.6	7.3	2i	NH_2CHO	17(0,17)–16(0,16)	345.1812	
345.2034	0.5	7.7	2i	U			
345.2266	0.6	10.6	2i	U			
345.2834	0.6	8.6	1i	$^{34}SO_2$	9(4,6)–9(3,7)	345.2857	
345.2916	0.6	9.4	1m	U			
345.3390	2.7	7.5	1m	SO_2	13(2,12)–12(1,11)	345.3385	
345.3352	3.1	6.0	2i	SO_2	13(2,12)–12(1,11)	345.3385	
345.3392	2.7	7.7	2i	$H^{13}CN$	4–3	345.3398	
345.3395	2.3	5.5	1m	$H^{13}CN$	4–3	345.3398	
345.4601	0.4	5.5	2i	U			
345.4681	0.5	9.1	2i	$HCOOCH_3$	28(13,15)–27(13,14)	345.4666	b
345.5215	0.5	8.4	2i	$^{34}SO_2$	7(4,4)–7(3,5)	345.5198	
345.5444	0.4	7.3	2i	U			
345.5524	0.5	7.6	2i	$^{34}SO_2$	6(4,2)–6(3,3)	345.5532	
345.6090	0.9	10.9	2i	HC_3N	38–37	345.6104	
345.6091	1.0	11.7	2i	HC_3N	38–37	345.6104	
345.6119	0.8	10.7	1m	HC_3N	38–37	345.6104	
345.7956	(25)	(20)	1i	CO	3–2	345.7959	self-absorbed
345.7941	(25)	(20)	2m	CO	3–2	345.7959	self-absorbed
345.9013	1.5	13.1	2i	CH_3OH	16(1)–15(2) $A-$	345.9042	
345.9043	1.1	9.7	1m	CH_3OH	16(1)–15(2) $A-$	345.9042	
345.9170	1.1	9.8	2i	CH_3OH	18(–3)–17(–4) E	345.9192	

Table 1. continued

ν(obs) (GHz)	T_A^* (K)	Width (MHz)	code	Species	Transition	ν(rest) (GHz)	Notes
345.9215	0.7	17.7	1m	CH_3OH	18(–3)–17(–4) E	345.9192	
346.2003	1.3	10.3	2i	CH_3OH	5(4)–6(3) $A-$	346.2028	
346.2032	1.3	8.0	2m	CH_3OH	5(4)–6(3) $A+$	346.2044	
346.2182	1.1	10.0	2i	U			
346.2213	1.2	8.0	2m	NS	(7.5,8.5)–(6.5,7.5)	346.2201	b
346.5087	0.3	7.0	1m	U			
346.5249	2.7	7.5	2i	SO	9(8)–8(7)	346.5286	
346.5280	3.1	9.8	2i	SO	9(8)–8(7)	346.5286	
346.5302	3.1	8.6	1m	SO	9(8)–8(7)	346.5286	
346.5983	0.8	7.6	2i	H_2CCO	17(1,16)–16(1,15)	346.6006	
346.6010	0.6	9.7	1m	H_2CCO	17(1,16)–16(1,15)	346.6006	
346.6489	1.1	8.7	2i	SO_2	19(1,19)–18(0,18)	346.6522	
346.6530	0.9	11.2	1m	SO_2	19(1,19)–18(0,18)	346.6522	
346.6515	0.9	8.4	2m	SO_2	19(1,19)–18(0,18)	346.6522	
346.6758	0.3	5.4	1m	$HCOOCH_3$	28(11,18)–17(11,17)	346.6748	b
346.6862	0.7	9.5	2i	U			
346.7146	0.7	13.5	2i	HCO	4(0,4)–3(0,3)	346.7252	?
346.9978	2.1	6.9	2m	$H^{13}CO^+$	4–3	346.9985	
346.9983	3.2	10.6	2i	$H^{13}CO^+$	4–3	346.9985	
347.0012	2.6	6.8	1m	$H^{13}CO^+$	4–3	346.9985	
347.1891	0.6	8.9	1m	U			in OMC1 (U347.191)
347.3257	0.7	12.7	2m	SiO	8–7	347.3306	
347.3313	0.6	10.1	1m	SiO	8–7	347.3306	
348.1027	0.4	11.1	1m	$^{13}CH_3OH$	10(1)–11(0) E	348.1003	
348.2026	0.3	10.5	1m	U			
348.2640	0.5	12.3	1m	HCOOD	16(8,8)–15(8,7)	348.2620	?
348.3305	0.5	10.1	1m	U			
348.3431	0.5	7.6	2m	$HN^{13}C$	4–3	348.3405	
348.3452	0.9	10.0	1m	$HN^{13}C$	4–3	348.3405	
348.3894	0.8	8.6	1m	SO_2	24(2,22)–23(3,21)	348.3880	
348.3900	0.5	8.4	2m	SO_2	24(2,22)–23(3,21)	348.3880	
348.5177	0.6	9.3	1m	HNO	1(1,1)–2(0,2)	348.5184	
348.5321	2.3	9.2	1m	H_2CS	10(1,9)–9(1,8)	348.5321	
348.6347	0.6	6.5	2m	H_2CCHCN	38(1,38)–37(10,37)	348.6357	
348.9128	0.7	10.8	2m	$HCOOCH_3$	28(9,20)–27(9,19)	348.9150	
349.1075	1.7	10.9	2m	CH_3OH	14(1)–14(0) $A+$,$A-$	349.1070	
349.1270	0.5	7.3	2m	CH_3CN	19(7)–18(7)	349.1234	
349.2139	1.0	8.0	2m	CH_3CN	19(6)–18(6)	349.2120	
349.2865	1.1	11.6	2m	CH_3CN	19(5)–18(5)	349.2858	
349.3406	1.5	8.0	2m	C_2H	4.5–3.5	349.3381	
349.3464	1.3	7.3	2m	CH_3CN	19(4)–18(4)	349.3462	
349.3936	1.2	8.0	2m	CH_3CN	19(3)–18(3)	349.3934	
349.4009	1.2	8.4	2m	C_2H	3.5–2.5	349.4006	
349.4270	1.1	9.5	2m	CH_3CN	19(2)–18(2)	349.4272	
349.4498	1.5	8.0	2m	CH_3CN	19(1)–18(1)	349.4471	
349.4564	1.3	7.7	2m	CH_3CN	19(0)–18(0)	349.4539	
349.8057	0.7	9.3	2m	$(CH_3)_2O$	10(1,10)–11(2,9)	349.8094	
349.8092	0.7	7.7	1m	$(CH_3)_2O$	10(1,10)–11(2,9)	349.8094	
349.8912	0.6	8.3	1m	U			
349.9554	0.5	6.9	2m	U			
350.1027	0.5	5.8	1m	$^{13}CH_3OH$	1(1)–0(0) $A+$	350.1031	
350.1046	0.6	10.6	2m	$^{13}CH_3OH$	1(1)–0(0) $A+$	350.1031	
350.1699	0.4	5.3	2m	U			
350.2869	1.1	7.3	2m	U			
350.3341	0.8	8.4	2m	HNCO	16(1,16)–15(1,15)	350.3333	
350.4480	0.6	8.0	2m	CH_3CN v8=1	18(–1)–17(–1) l=1	350.4495	
350.5559	0.6	9.8	2m	CH_3CN v8=1	18(2)–17(2) l=1	350.5522	
350.6867	0.5	8.7	1i	CH_3OH	4(0)–3(–1) E	350.6877	
350.6866	3.3	9.5	2m	CH_3OH	4(0)–3(–1) E	350.6877	

Table 1. continued

ν(obs) (GHz)	T_A^* (K)	Width (MHz)	code	Species	Transition	ν(rest) (GHz)	Notes
350.8044	2.5	7.3	2m	U			
350.8471	0.9	9.8	2m	U			
350.8660	0.7	9.1	2m	SO_2	10(6,4)–11(5,7)	350.8629	
350.9045	0.6	10.3	1i	CH_3OH	1(1)–0(0) $A+$	350.9051	
350.9045	2.7	6.9	2m	CH_3OH	1(1)–0(0) $A+$	350.9051	
351.0136	0.4	11.0	1i	$HCOOCH_3$	28(7,22)–27(7,21)	351.0158	
351.0160	0.6	9.8	2m	$HCOOCH_3$	28(7,22)–27(7,21)	351.0158	
351.0472	0.4	11.2	1i	NO	3.5,4.5–2.5,3.5	351.0435	
351.0541	0.6	10.2	2m	NO	3.5,3.5–2.5,2.5	351.0517	
351.2357	1.0	10.1	1i	CH_3OH	10(4)–9(5) E	351.2367	
351.2371	1.2	8.7	2m	CH_3OH	10(4)–9(5) E	351.2367	
351.2589	1.1	9.8	2m	SO_2	5(3,3)–4(2,2)	351.2572	
351.4201	0.4	7.3	2m	U			
351.4561	0.7	6.9	2m	H_2CNH	10(1,9)–10(0,10)	351.4536	
351.4649	0.7	8.6	2m	$O^{13}CS$	29–28	351.4650	
351.4663	0.7	6.0	1i	$O^{13}CS$	29–28	351.4650	
351.5394	0.7	7.8	1i	U			
351.5539	0.5	8.5	1i	U			
351.6362	0.7	7.6	2m	HNCO	16(0,16)–15(0,15)	351.6335	
351.7705	4.2	6.5	1i	H_2CO	5(1,5)–4(1,4)	351.7686	
351.7709	6.1	7.3	2m	H_2CO	5(1,5)–4(1,4)	351.7686	
351.8227	0.3	9.4	1i	U			
351.8728	1.1	10.0	1i	SO_2	14(4,10)–14(3,11)	351.8739	
351.8754	0.7	6.5	2m	SO_2	14(4,10)–14(3,11)	351.8739	
351.9191	0.3	9.6	1i	C_2H_5OH	25(3,22)–24(4,21)	351.9180	
352.2778	0.4	5.5	2m	U			
352.4052	0.7	11.3	2m	U			
352.5945	1.8	10.2	2m	OCS	29–28	352.5996	
353.7292	0.7	18.7	1i	$HCOOCH_3$	32(1,31)–31(1,30)	353.7289	
354.1224	0.6	6.5	2m	U			
354.4615	0.8	12.5	1i	HCN	4–3 $(0,1^{1c},0)$	354.4610	
354.4968	2.0	10.6	1i	U			
354.5052	9.1	5.5	2m	HCN	4–3	354.5055	
354.5090	7.1	5.4	1i	HCN	4–3	354.5055	
354.5465	0.3	5.7	1i	U			
354.5768	0.4	2.1	1i	U			
354.6073	0.8	9.1	2m	$HCOOCH_3$	33(0,33)–32(0,32)	354.6082	b
354.6074	0.7	8.4	1i	$HCOOCH_3$	33(0,33)–32(0,32)	354.6082	b
354.6974	0.9	9.1	2m	HC_3N	39–38	354.6987	
354.8450	0.6	8.0	2m	U			
355.0468	0.7	6.4	1i	SO_2	12(4,8)–12(3,9)	355.0455	
355.1558	0.3	7.6	1i	SO_2	32(2,30)–33(1,33)	355.1536	
355.1854	0.4	5.0	1i	SO_2	17(4,14)–18(1,17)	355.1864	
355.2782	0.5	3.6	1i	U			
355.6025	1.5	10.9	2i	CH_3OH	13(0)–12(1) $A+$	355.6030	
355.9659	0.4	9.4	2m	CH_3OH	16(3)–16(2) E vt1	355.9644	
355.9906	0.4	6.9	2i	U			
356.0062	2.1	9.1	2i	CH_3OH	15(1)–15(0) $A+$	356.0066	
356.0074	1.8	9.9	1i	CH_3OH	15(1)–15(0) $A+$	356.0066	
356.0074	1.8	9.9	1i	CH_3OH	15(1)–15(0) $A+$	356.0066	
356.2553	0.6	8.7	2m	HCN	4–3 $(0,1^{1d},0)$	356.2560	
356.2555	0.6	15.6	1i	HCN	4–3 $(0,1^{1d},0)$	356.2560	
356.2936	0.4	6.9	1i	U			$HCOOCH_3$?
356.4008	0.5	6.0	1i	U			$HCOOCH_3$?
356.5777	0.7	7.7	2i	U			
356.5835	0.7	7.3	2i	U			
356.7306	(10)	(15)	2i	HCO^+	4–3	356.7342	self-absorbed
357.0665	0.5	9.1	2i	CH_3OD	8(1)–7(1) $A+$	357.0662	b
				C_2H_5OH	10(4,7)–9(3,6)	357.0670	*
357.1667	0.6	7.3	2i	SO_2	13(4,10)–13(3,11)	357.1654	

Table 1. continued

ν(obs) (GHz)	T_A^* (K)	Width (MHz)	code	Species	Transition	ν(rest) (GHz)	Notes
357.2156	0.5	12.2	2i	U			
357.2397	1.0	13.0	2i	SO_2	15(4,12)–15(3,13)	357.2412	
357.3900	1.0	10.6	2i	SO_2	11(4,8)–11(3,9)	357.3876	
357.3944	0.6	9.0	2i	SO_2	11(4,8)–11(3,9)	357.3876	
357.4612	0.8	9.0	2i	U			
357.5516	0.5	6.6	2i	$HCOOCH_3$	29(14,16)–28(14,15)	357.5492	b
357.5814	0.6	10.5	2i	SO_2	8(4,4)–8(3,5)	357.5815	
357.6591	0.7	9.5	2i	$^{13}CH_3OH$	7(2)–6(1) E	357.6580	
357.6722	0.9	9.5	2i	SO_2	9(4,6)–9(3,7)	357.6719	
357.6730	0.6	8.1	1i	SO_2	9(4,6)–9(3,7)	357.6719	
357.6816	0.6	9.4	2i	C_2H_5OH	7(5,3)–6(4,2)	357.6810	b
				C_2H_5OH	7(5,2)–6(4,3)	357.6820	
357.8939	0.8	6.6	1i	SO_2	7(4,4)–7(3,5)	357.8925	
357.8944	0.8	8.4	2i	SO_2	7(4,4)–7(3,5)	357.8925	
357.9259	0.9	8.0	1i	SO_2	6(4,2)–6(3,3)	357.9259	
357.9289	0.9	9.1	2i	SO_2	6(4,2)–6(3,3)	357.9259	
357.9636	0.7	8.1	1i	SO_2	17(4,14)–17(3,15)	357.9629	
357.9641	0.7	9.8	2i	SO_2	17(4,14)–17(3,15)	357.9629	
357.9941	0.7	9.4	1i	CH_3OH	15(3)–15(2) E vt1	357.9941	*
				$HCOOCH_3$	29(13,17)–28(13,16)	357.9951	
357.9957	1.2	8.2	2i	CH_3OH	15(3)–15(2) E vt1	357.9941	*
				$HCOOCH_3$	29(13,17)–28(13,16)	357.9951	
358.0150	1.1	10.2	2i	SO_2	5(4,2)–5(3,3)	358.0132	
358.0382	0.7	9.8	2i	SO_2	4(4,0)–4(3,1)	358.0380	
358.0399	0.4	8.0	1i	SO_2	4(4,0)–4(3,1)	358.0380	
358.2157	0.6	9.5	2i	SO_2	20(0,20)–19(1,19)	358.2157	
358.4532	1.5	11.4	2i	U			
358.5756	1.1	10.2	2i	$HCOOCH_3$	29(12,18)–28(12,17)	358.5762	b
358.6064	3.2	9.4	2i	CH_3OH	4(1)–3(0) E	358.6058	
358.7285	0.6	7.3	2i	U			
358.8163	0.6	8.0	2i	U			
358.9903	0.5	6.2	2i	U			
359.0048	0.8	7.6	2i	U			
359.1522	0.7	10.9	2i	SO_2	25(3,23)–25(2,24)	359.1512	
359.3868	0.8	7.3	2i	$(CH_3)_2O$	11(2,9)–12(3,10)	359.3846	
359.5447	0.6	12.8	2i	U			
359.5582	0.7	8.7	2i	$HCOOCH_3$	29(6,24)–28(6,23)	359.5581	
359.7705	0.6	8.4	2i	SO_2	19(4,16)–19(3,17)	359.7707	

Table 2. Rotation temperatures, molecular column densities and abundances relative to H_2. The average molecular hydrogen column density over the 14″ beam area has been assumed to be 5.3 10^{23} cm^{-2} (Millar et al. 1995)

Species	$T_{\rm rot}$ (K)	N (cm^{-2})	X	Notes	Figure 6
H_2CCO	273±10	$6.7\pm5.7\times10^{14}$	1.3×10^{-9}	3 points (1 line blended with C_2H_5OH)	a
CH_3OH	368±16	$1.8\pm0.2\times10^{16}$	3.4×10^{-8}	A-type	b
CH_3OH	336±14	$1.9\pm0.1\times10^{16}$	3.6×10^{-8}	E-type	c
$^{13}CH_3OH$	64±15	$5.6\pm5.3\times10^{14}$	1.1×10^{-9}	A-type; 3 points	d
$HCOOCH_3$	147±10	$1.6\pm0.1\times10^{16}$	3.0×10^{-8}	$E_u < 400$ K	e
CH_3CN	359±73	$2.4\pm1.0\times10^{14}$	4.5×10^{-10}	J=19–18 only	f
H_2CCHCN	74±5	$4.1\pm2.1\times10^{15}$	7.7×10^{-9}	–	g
NH_2CHO	–	–	–	–	h
SO	22±2	$9.1\pm4.5\times10^{14}$	1.7×10^{-9}	–	i
SO_2	108±4	$1.6\pm0.2\times10^{15}$	3.0×10^{-9}	$E_u < 250$ K	j
	284±21	$2.5\pm1.2\times10^{15}$	4.7×10^{-9}	$E_u > 250$ K	
$^{34}SO_2$	131±65	$8.6\pm8.6\times10^{14}$	1.6×10^{-9}	–	k
H_2CS	243±35	$1.2\pm0.4\times10^{15}$	2.3×10^{-9}	–	l
C_2H_5OH	94±27	$3.5\pm2.0\times10^{15}$	6.6×10^{-9}	(1 line blended with H_2CCO)	m
CH_3CCH	93±66	$1.8\pm1.8\times10^{16}$	3.4×10^{-8}	–	n

Table 3. Assumed rotation temperature and associated lower limit to molecular column density and abundance relative to H_2 for molecules with only one or two detected lines (see Sect. 3.2). The average molecular hydrogen column density over the 14″ beam area has been assumed to be 5.3 10^{23} cm^{-2} (Millar et al. 1995). Where two independent lines have been detected, values for $T_{\rm rot}$ and N are given for each transition in order of increasing frequency. In some cases, the quoted values are for the sum over all hyperfines

Species	$T_{\rm rot}$ (K)	$N_{\rm min}$ (cm^{-2})	$X_{\rm min}$	Species	$T_{\rm rot}$ (K)	$N_{\rm min}$ (cm^{-2})	$X_{\rm min}$
$C^{17}O$	32	1.2×10^{16}	2.3×10^{-8}	HC_3N	307	1.2×10^{13}	2.3×10^{-11}
C_2H	42	8.1×10^{15}	1.5×10^{-8}		324	2.5×10^{13}	4.7×10^{-11}
HDO	224	2.1×10^{15}	4.0×10^{-9}	NO	39	5.8×10^{15}	1.1×10^{-8}
HCO	183	5.3×10^{13}	1.0×10^{-10}	HNO	19	2.4×10^{14}	4.6×10^{-10}
	28	1.2×10^{13}	2.3×10^{-11}	HNCO	124	2.8×10^{14}	5.3×10^{-10}
$H^{13}CO^+$	42	1.2×10^{13}	2.3×10^{-11}		96	1.5×10^{14}	2.8×10^{-10}
$HC^{18}O^+$	41	4.1×10^{12}	2.3×10^{-12}	H_2CNH	122	4.2×10^{14}	7.9×10^{-10}
$D^{13}CO^+$	51	2.7×10^{12}	5.1×10^{-12}	C_2H_5CN	219	4.7×10^{14}	8.9×10^{-10}
H_2CO	42	1.7×10^{14}	3.2×10^{-10}	CS	66	8.4×10^{13}	1.6×10^{-10}
$H_2{}^{13}CO$	41	7.4×10^{13}	1.4×10^{-10}	$C^{34}S$	65	6.4×10^{13}	1.2×10^{-10}
	66	3.8×10^{14}	7.2×10^{-10}	$C^{33}S$	65	4.7×10^{13}	8.9×10^{-11}
HCOOH	97	9.1×10^{14}	1.7×10^{-9}	^{34}SO	81	1.2×10^{14}	2.3×10^{-10}
HCOOD	208	3.5×10^{15}	6.6×10^{-9}	NS	71	4.0×10^{13}	7.5×10^{-11}
$H^{13}COOH$	84	7.0×10^{14}	1.3×10^{-9}	HCS^+	74	3.0×10^{13}	5.6×10^{-11}
$^{13}CH_3OH$–E	108	1.6×10^{15}	3.1×10^{-9}	OCS	237	1.3×10^{15}	2.5×10^{-9}
	57	9.7×10^{14}	1.8×10^{-9}		254	1.6×10^{15}	3.0×10^{-9}
CH_3OD	56	5.9×10^{14}	1.1×10^{-9}	$O^{13}CS$	253	4.8×10^{14}	9.1×10^{-10}
CN	33	5.9×10^{14}	1.1×10^{-9}	$OC^{34}S$	248	4.3×10^{14}	8.1×10^{-10}
HCN	42	3.8×10^{13}	7.2×10^{-11}	$H_2{}^{13}CS$	137	3.2×10^{14}	6.0×10^{-10}
$H^{13}CN$	41	1.5×10^{13}	2.8×10^{-11}	$H_2C^{34}S$	200	3.1×10^{15}	5.8×10^{-9}
$HC^{15}N$	41	1.6×10^{13}	3.0×10^{-11}	SHD	23	1.1×10^{14}	2.1×10^{-10}
$HN^{13}C$	42	5.5×10^{12}	1.0×10^{-11}	SiO	75	1.2×10^{13}	2.3×10^{-11}

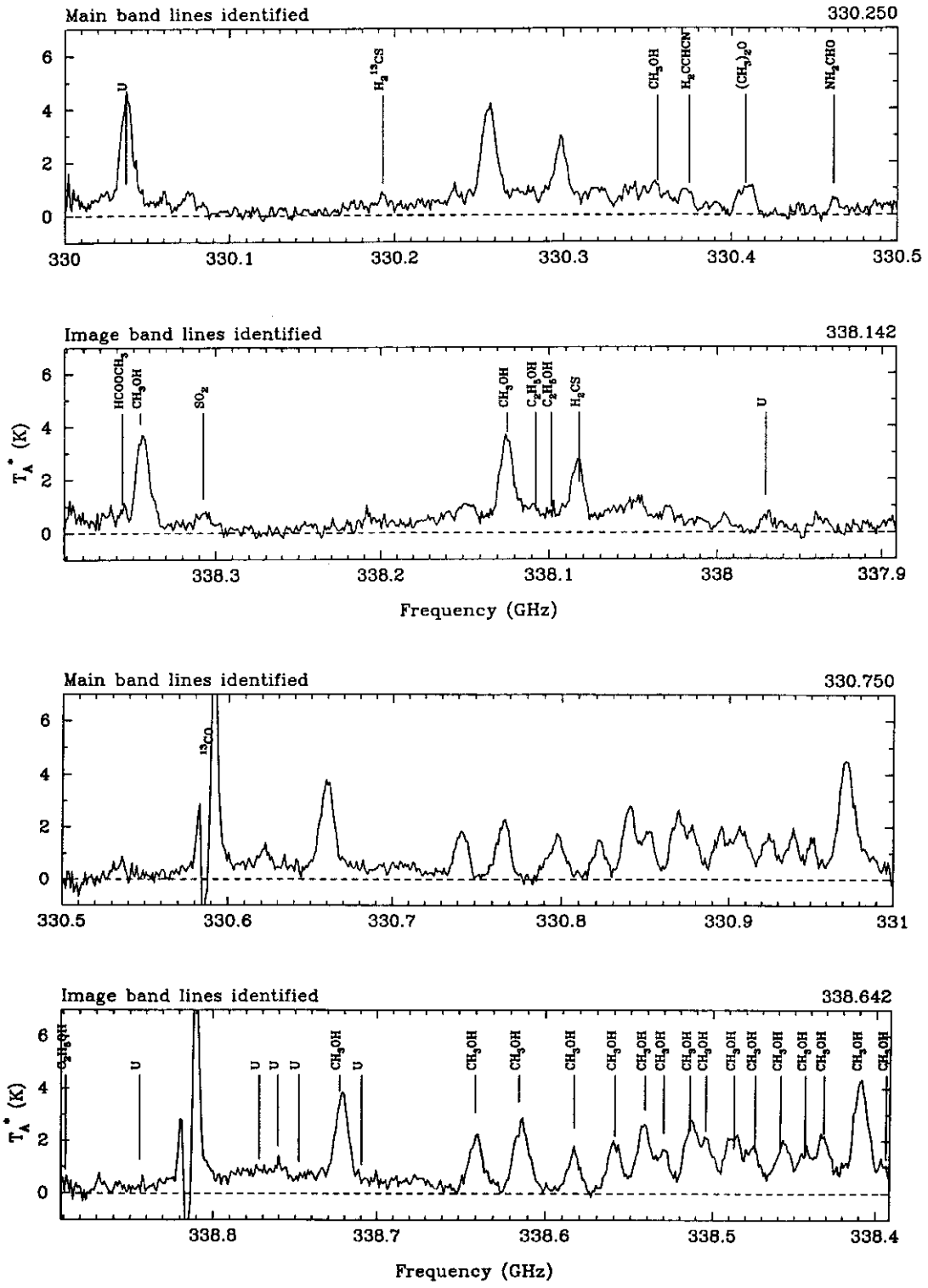

Fig. 4. Spectra of emission from G 34.3+0.15 over 330−360 GHz frequency range. Each spectrum is 500 MHz wide, with resolution reduced by binning to 1 MHz. Spectra are arranged in pairs, with the lower panel showing the same spectral range as the upper panel but with the local oscillator shifted by +10 MHz. Centre frequency in GHz for each spectrum is given in the top right corner. Spectral lines identified in the upper panel are in the 'main' sideband, those given in the lower are in the 'image' sideband. Consequently, the frequency scale runs in opposite directions on the two spectra. The intensity scale is T_A^* in K; the frequency scale is in GHz

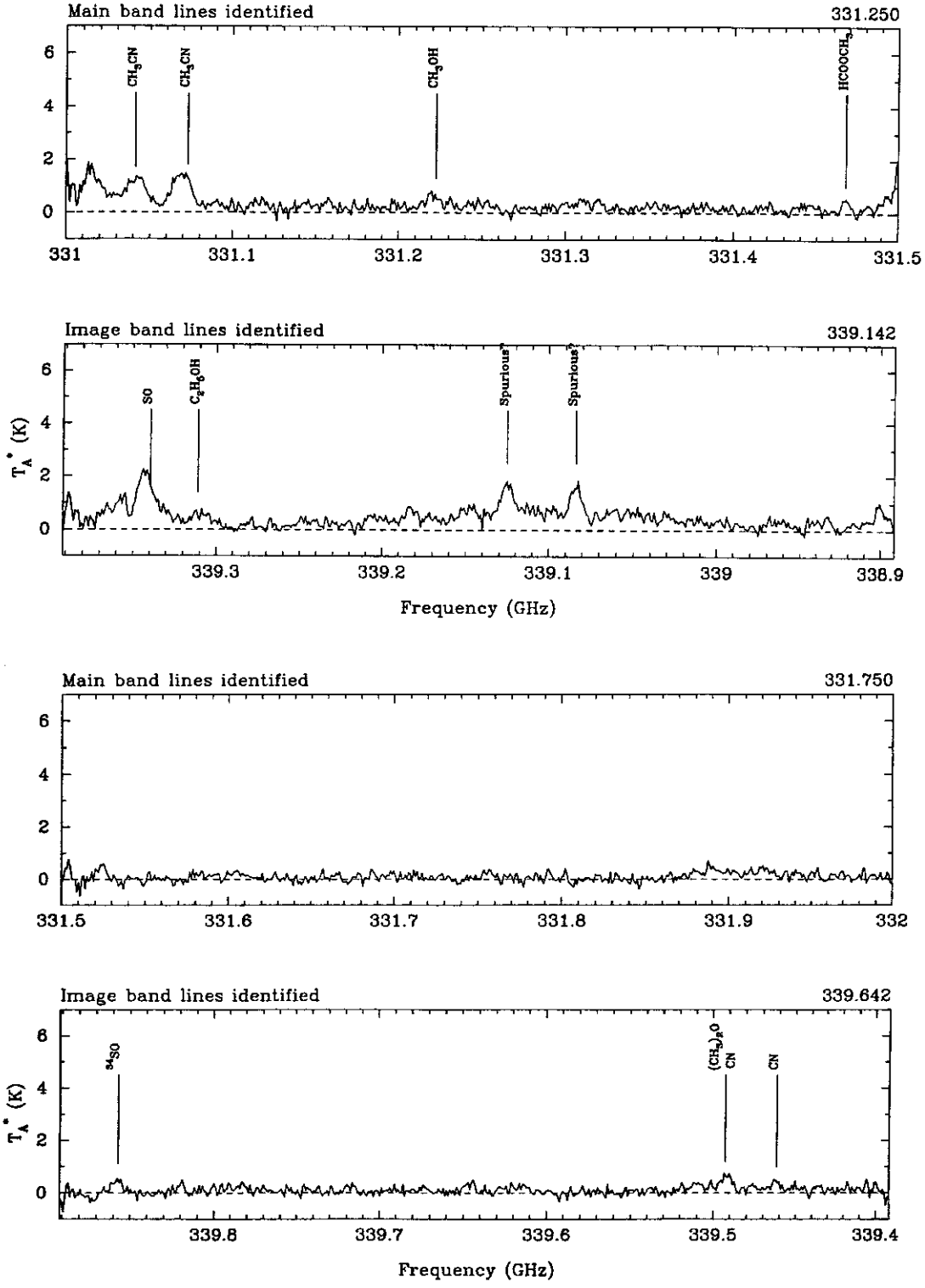

Fig. 4. continued

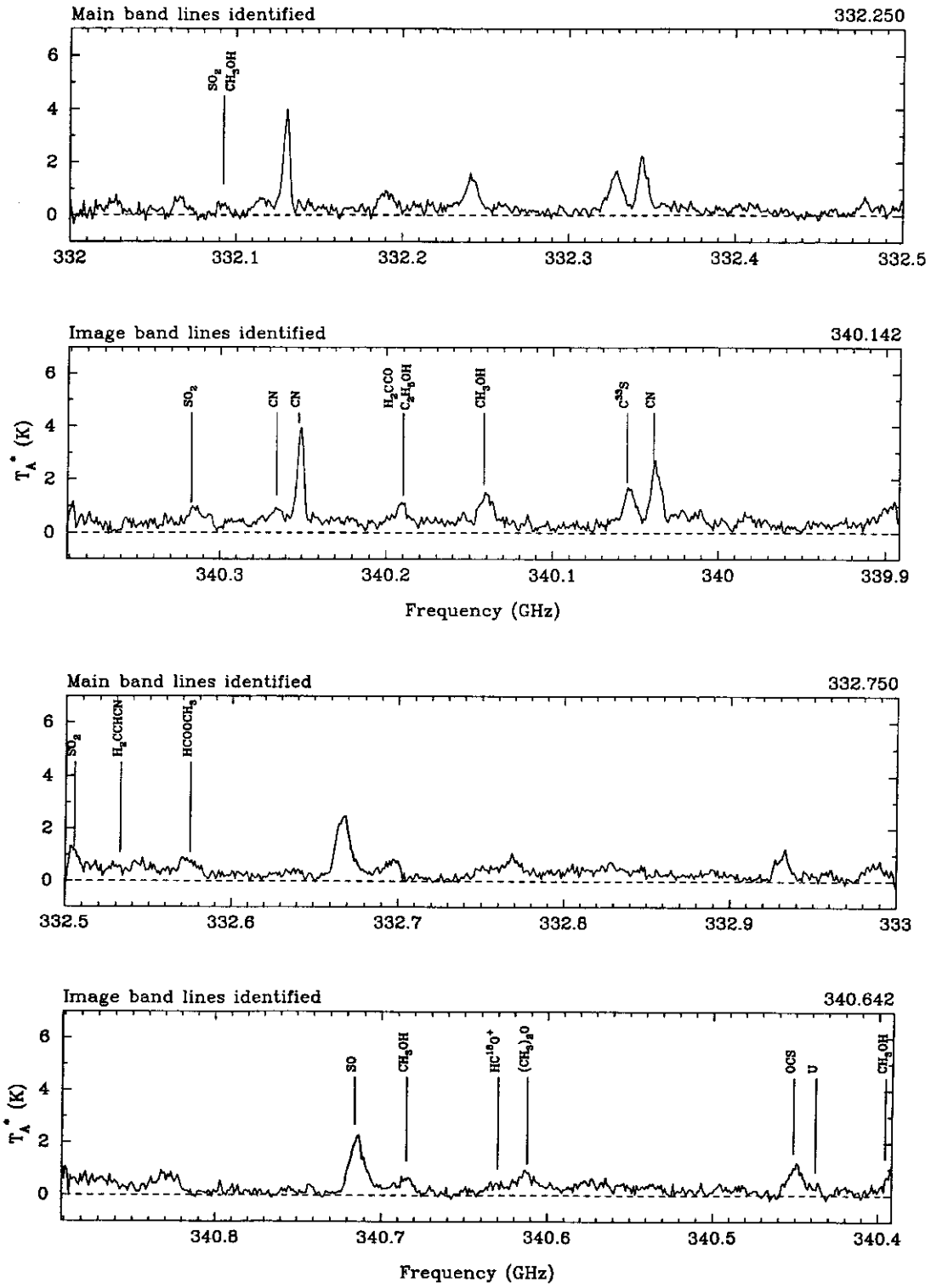

Fig. 4. continued

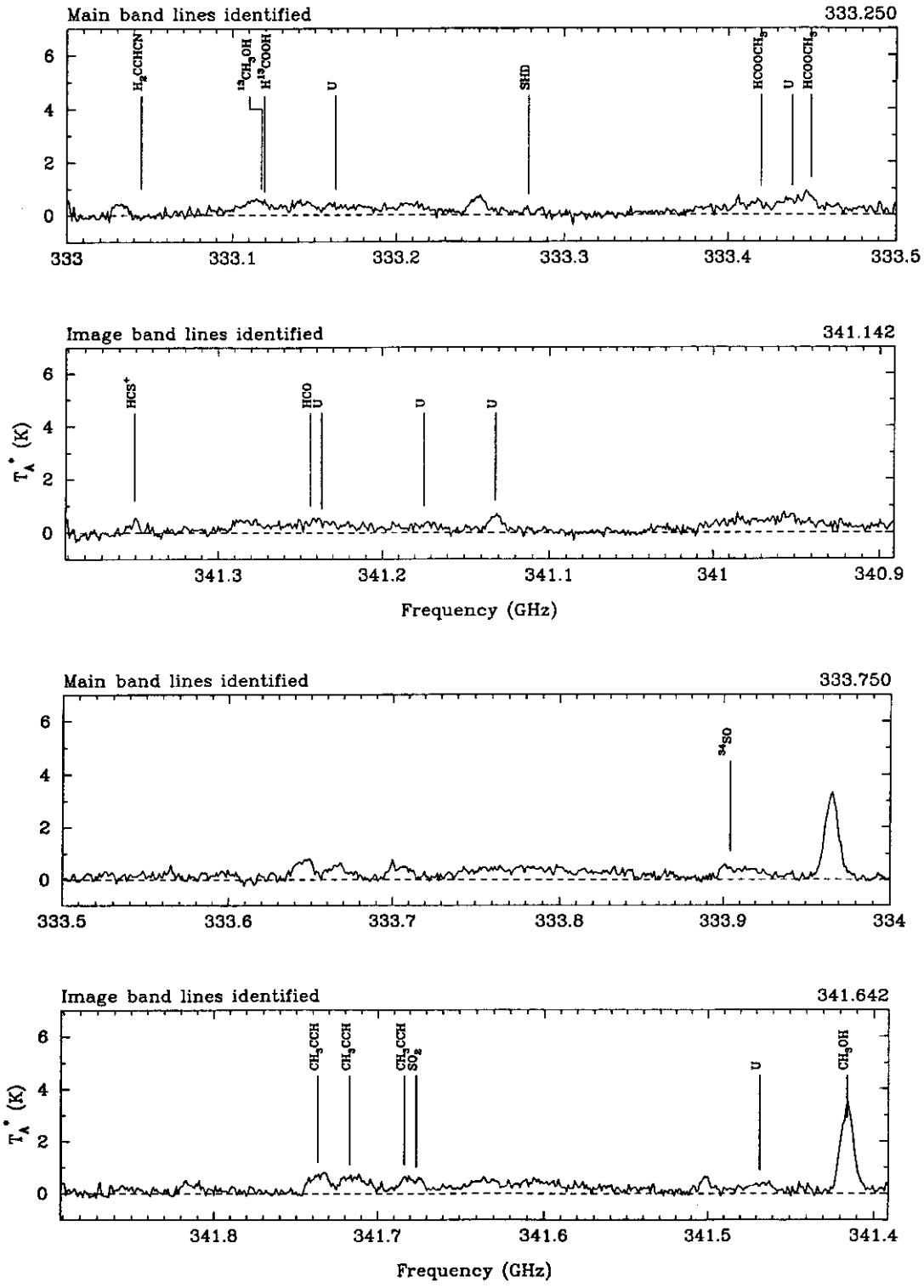

Fig. 4. continued

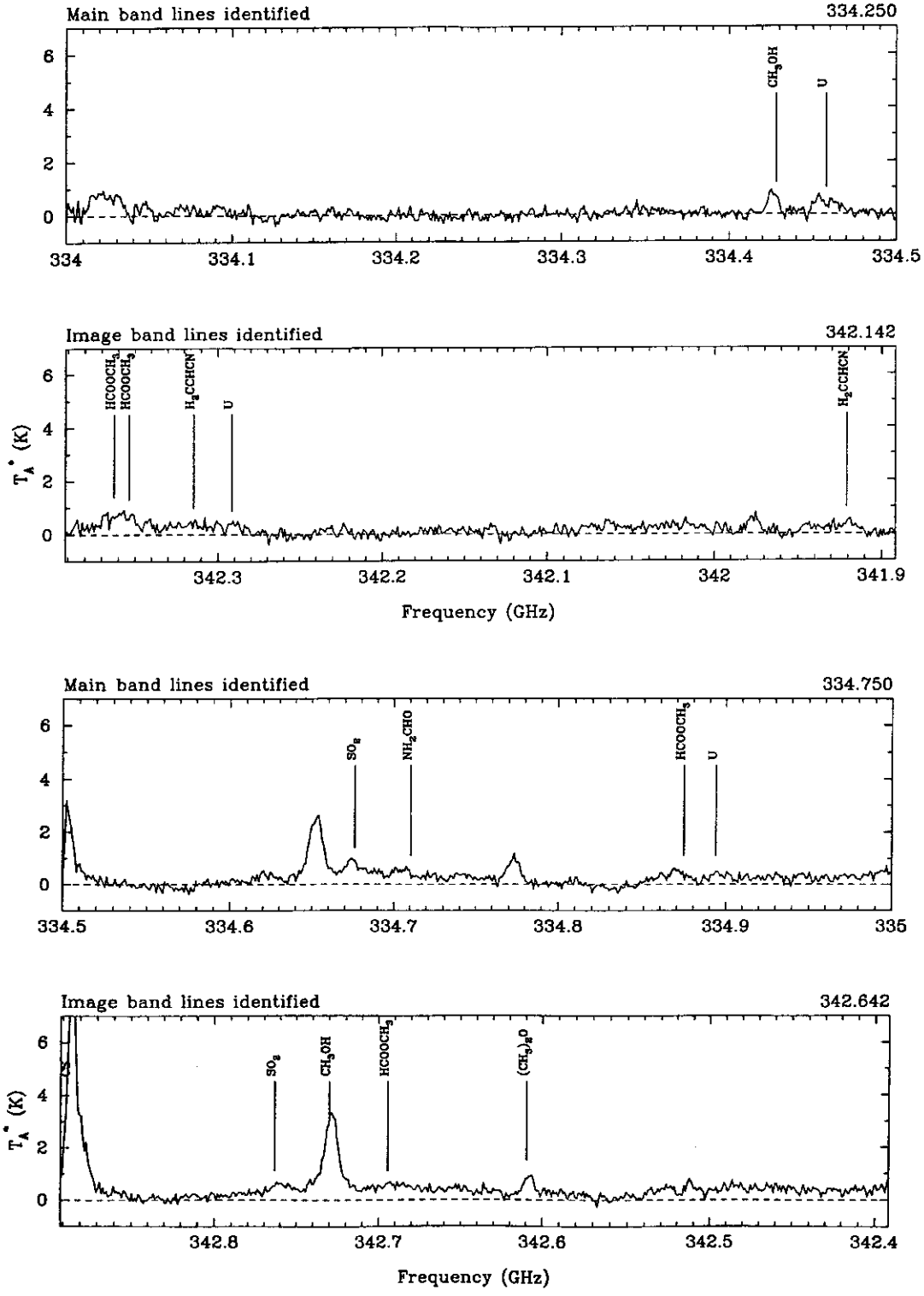

Fig. 4. continued

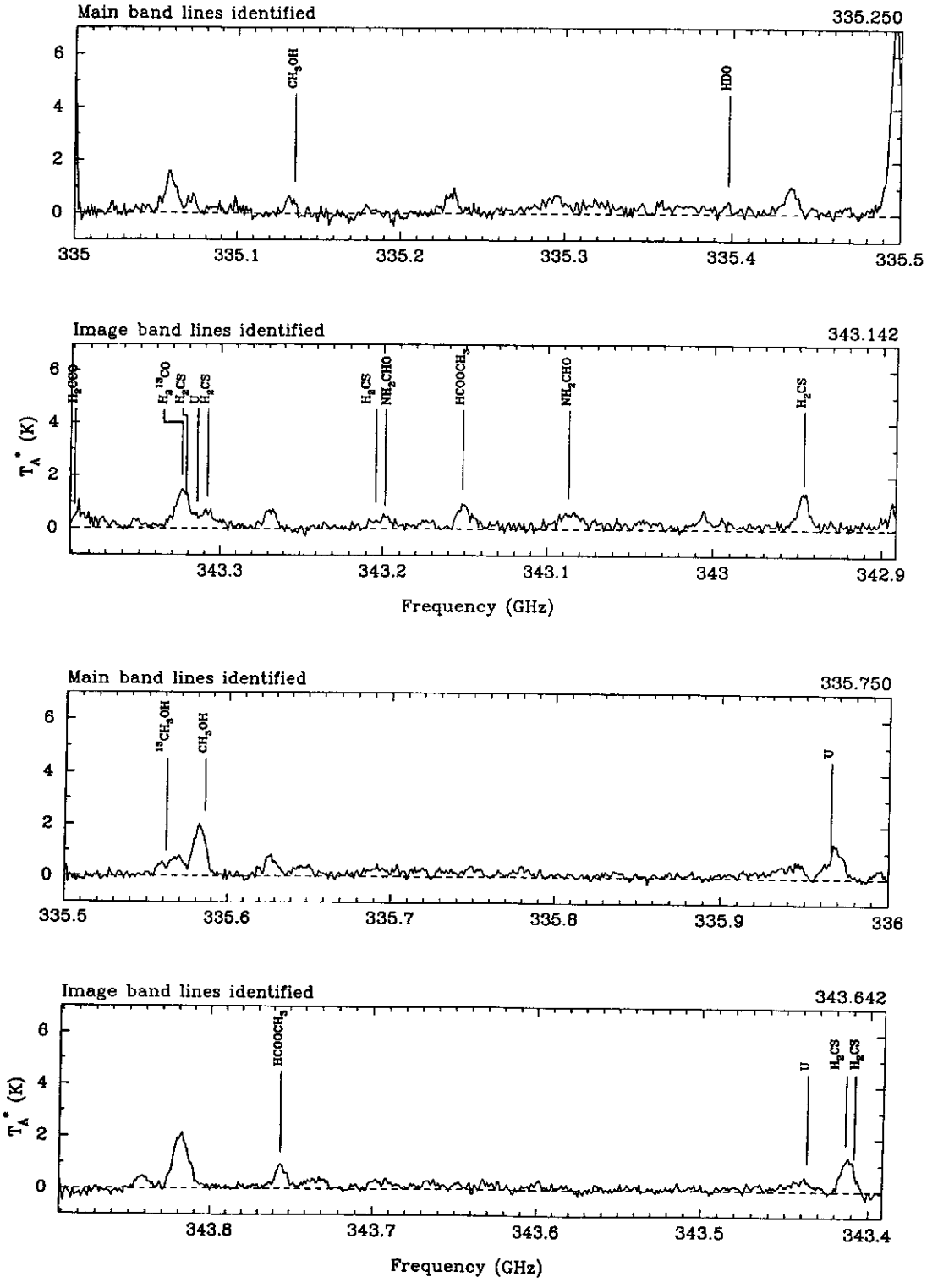

Fig. 4. continued

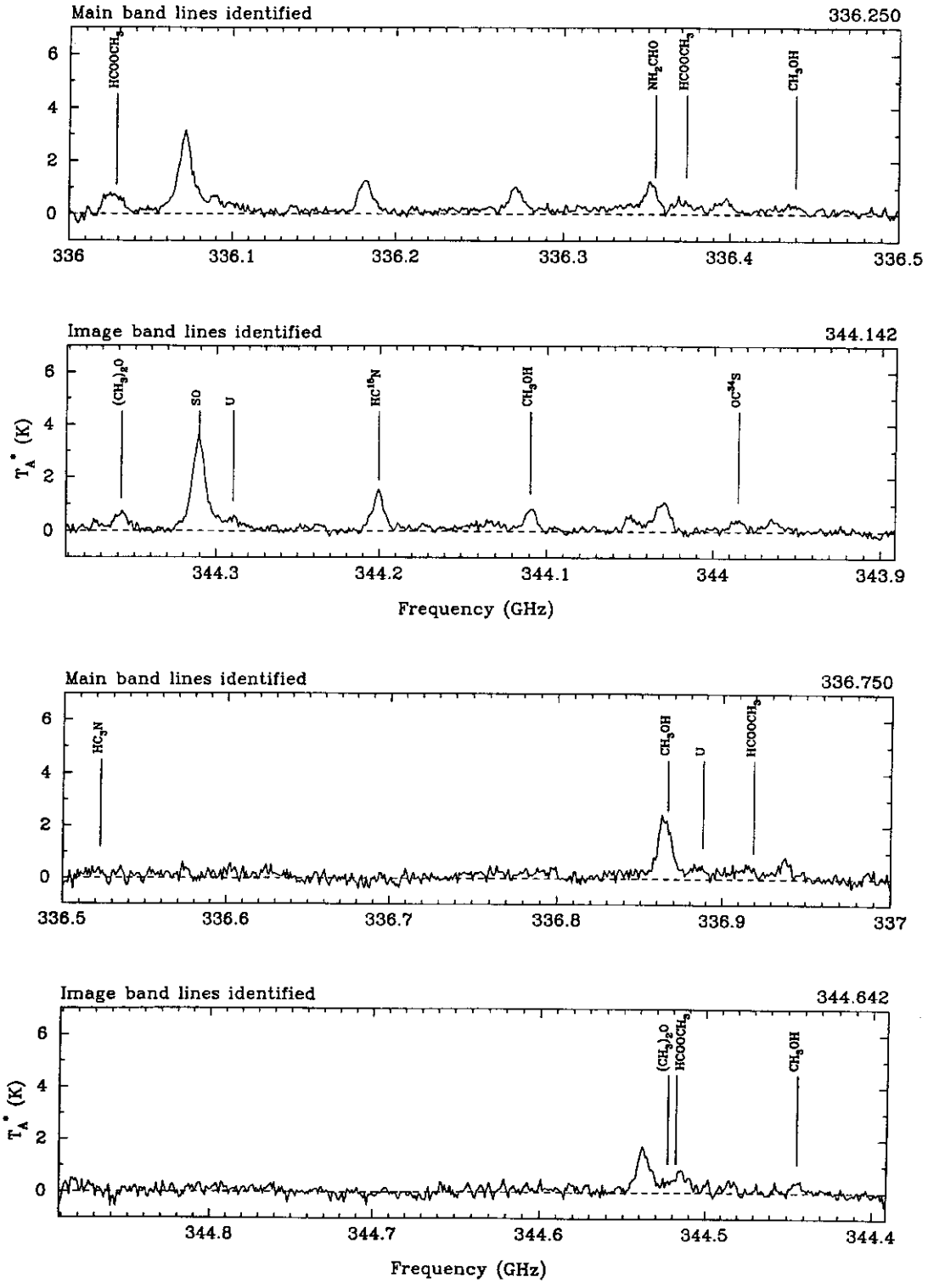

Fig. 4. continued

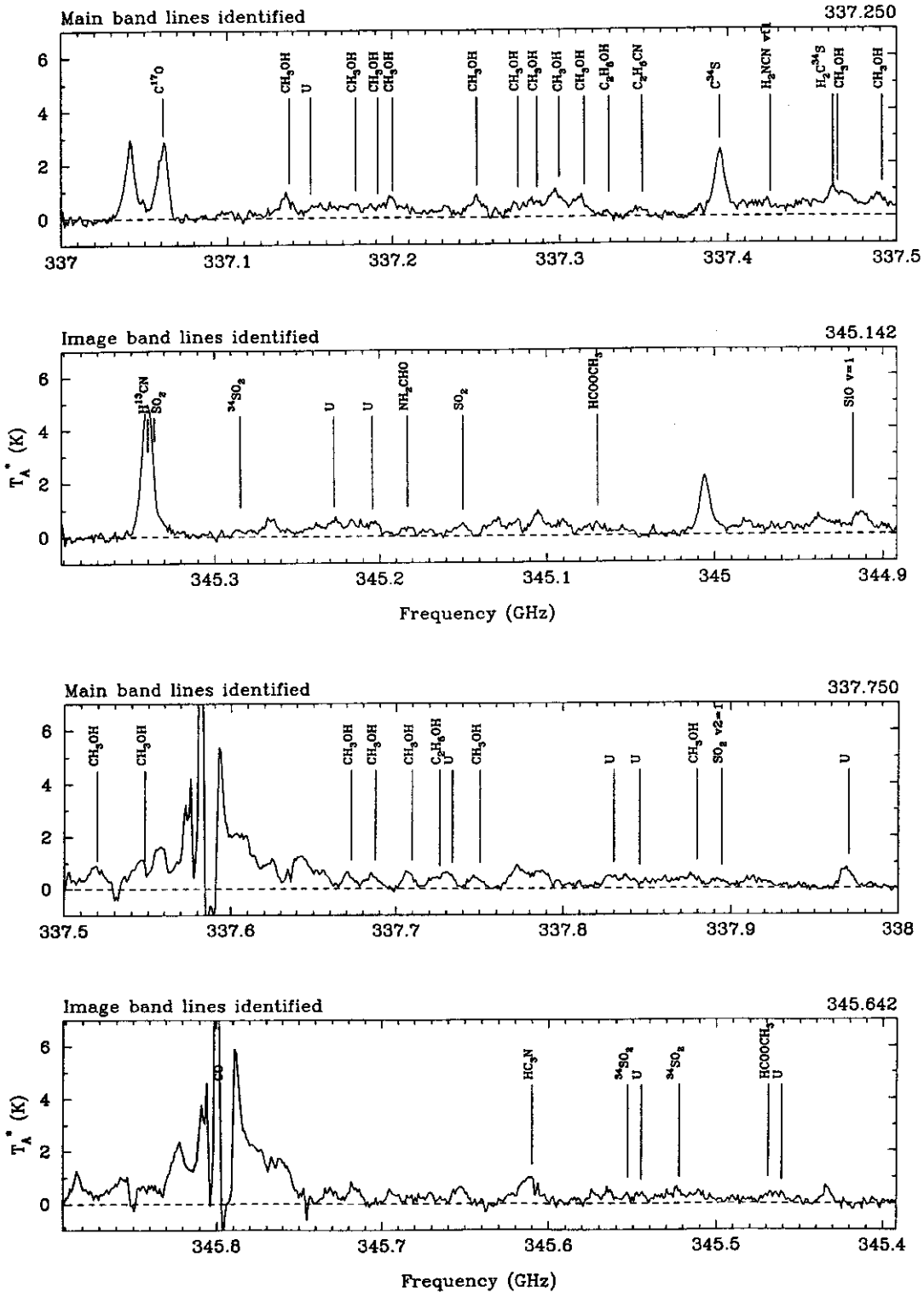

Fig. 4. continued

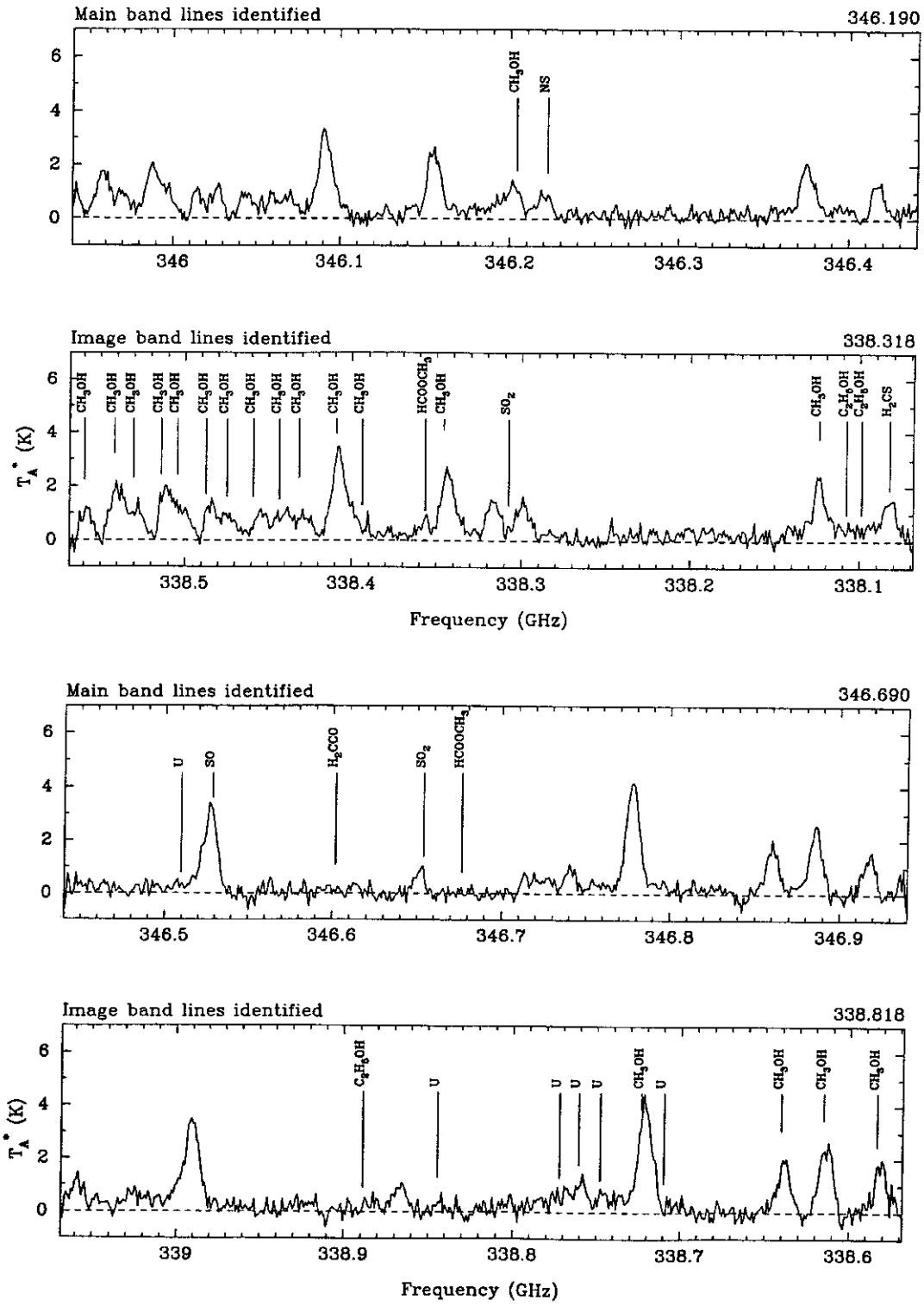

Fig. 4. continued

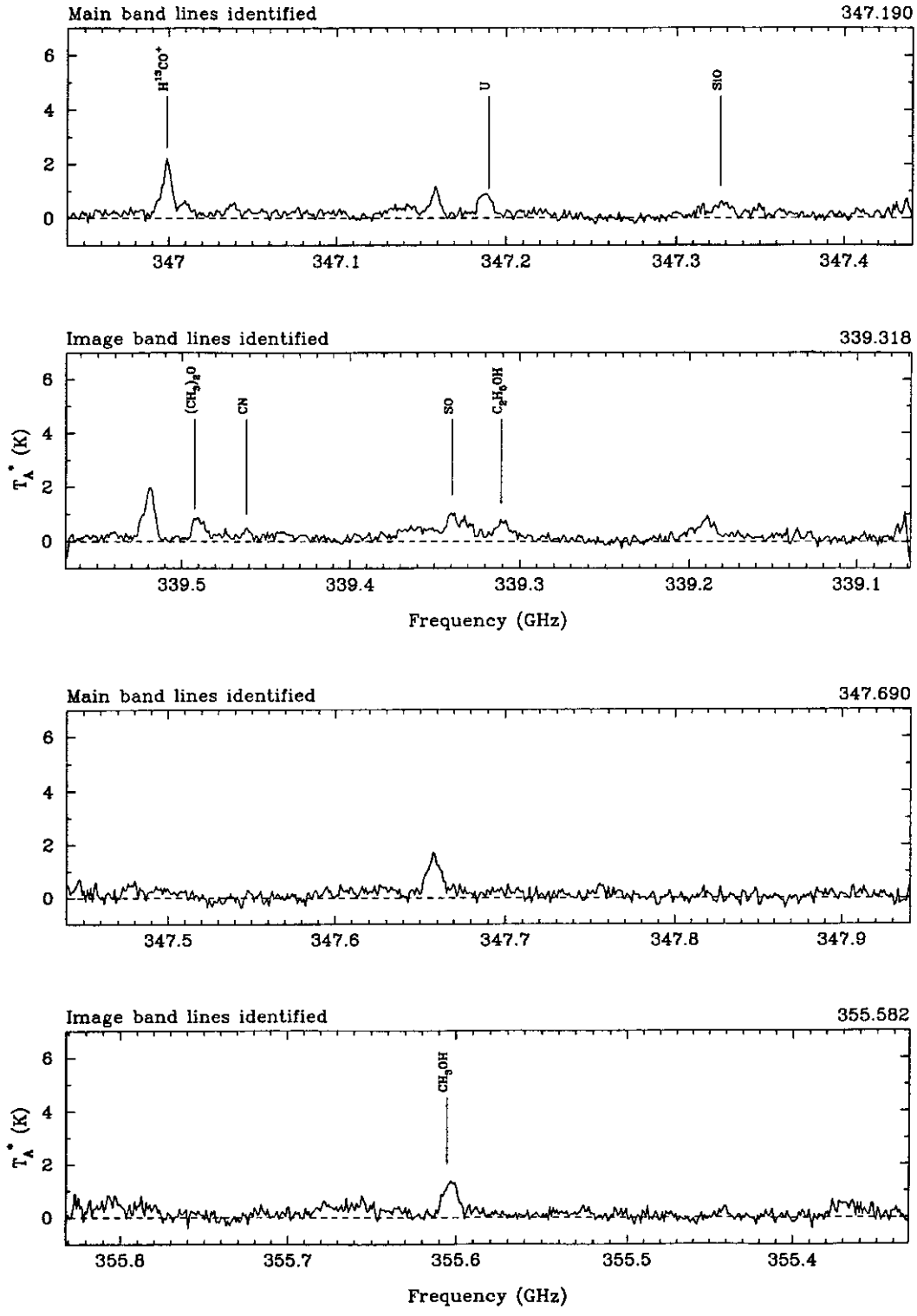

Fig. 4. continued

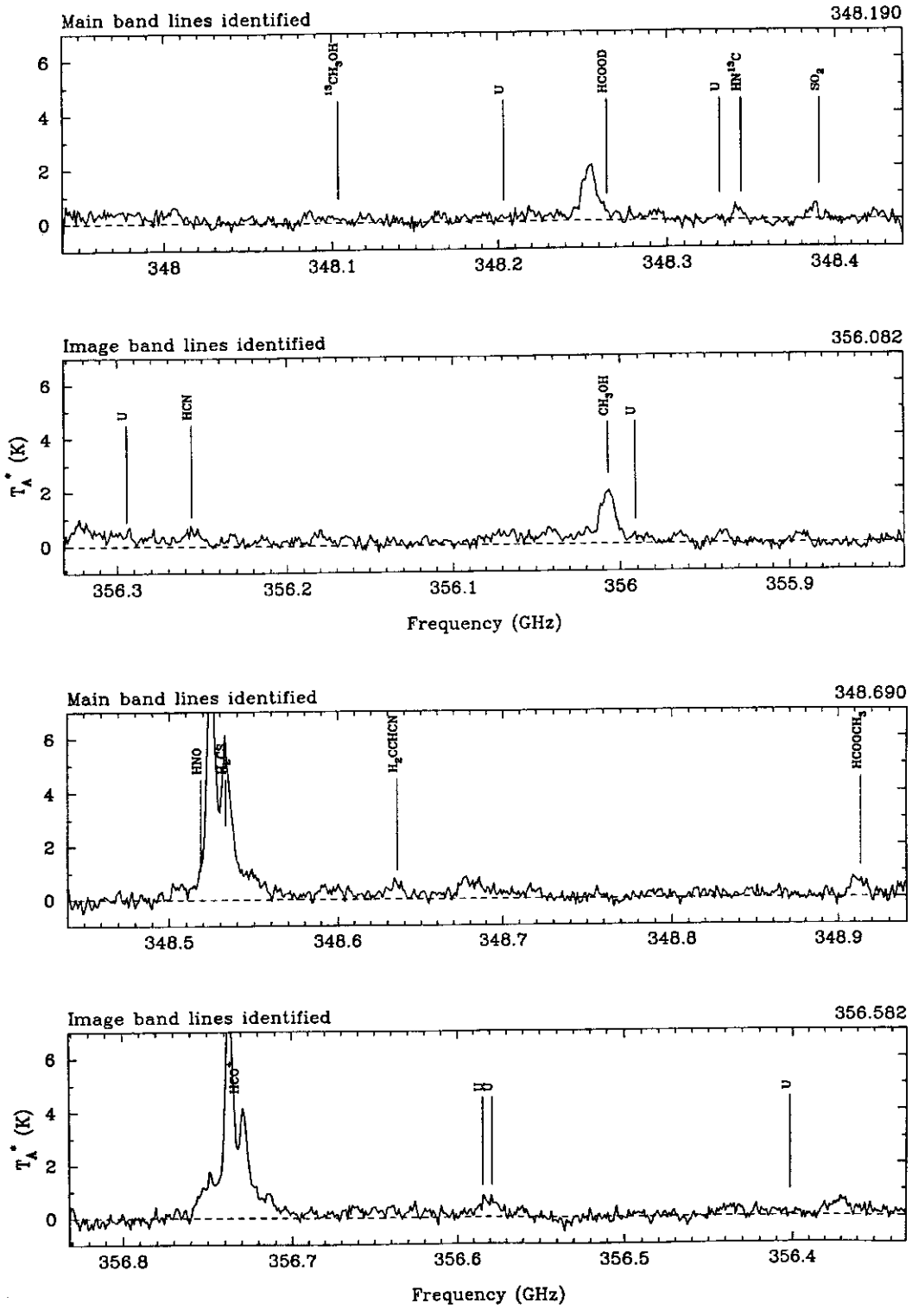

Fig. 4. continued

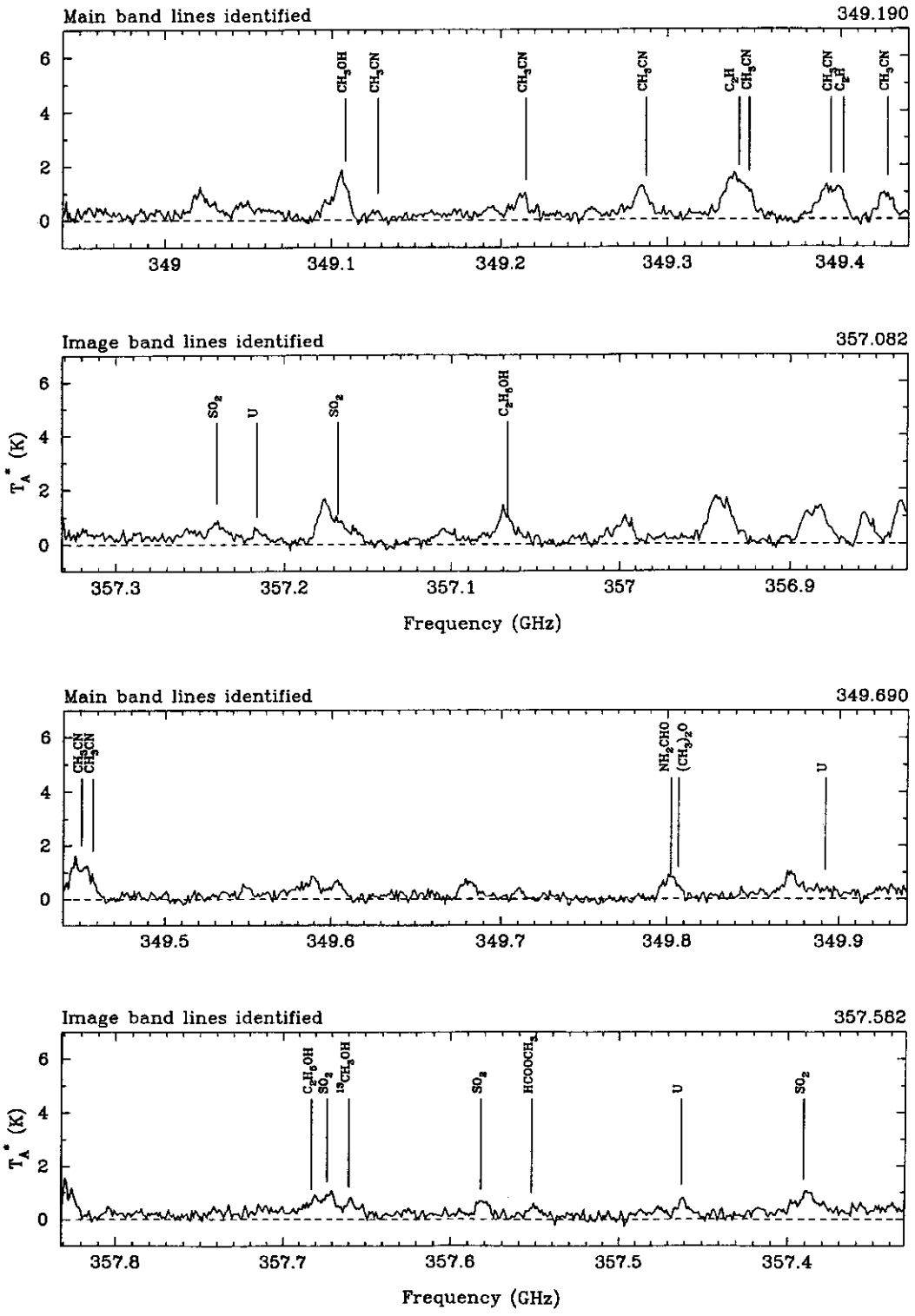

Fig. 4. continued

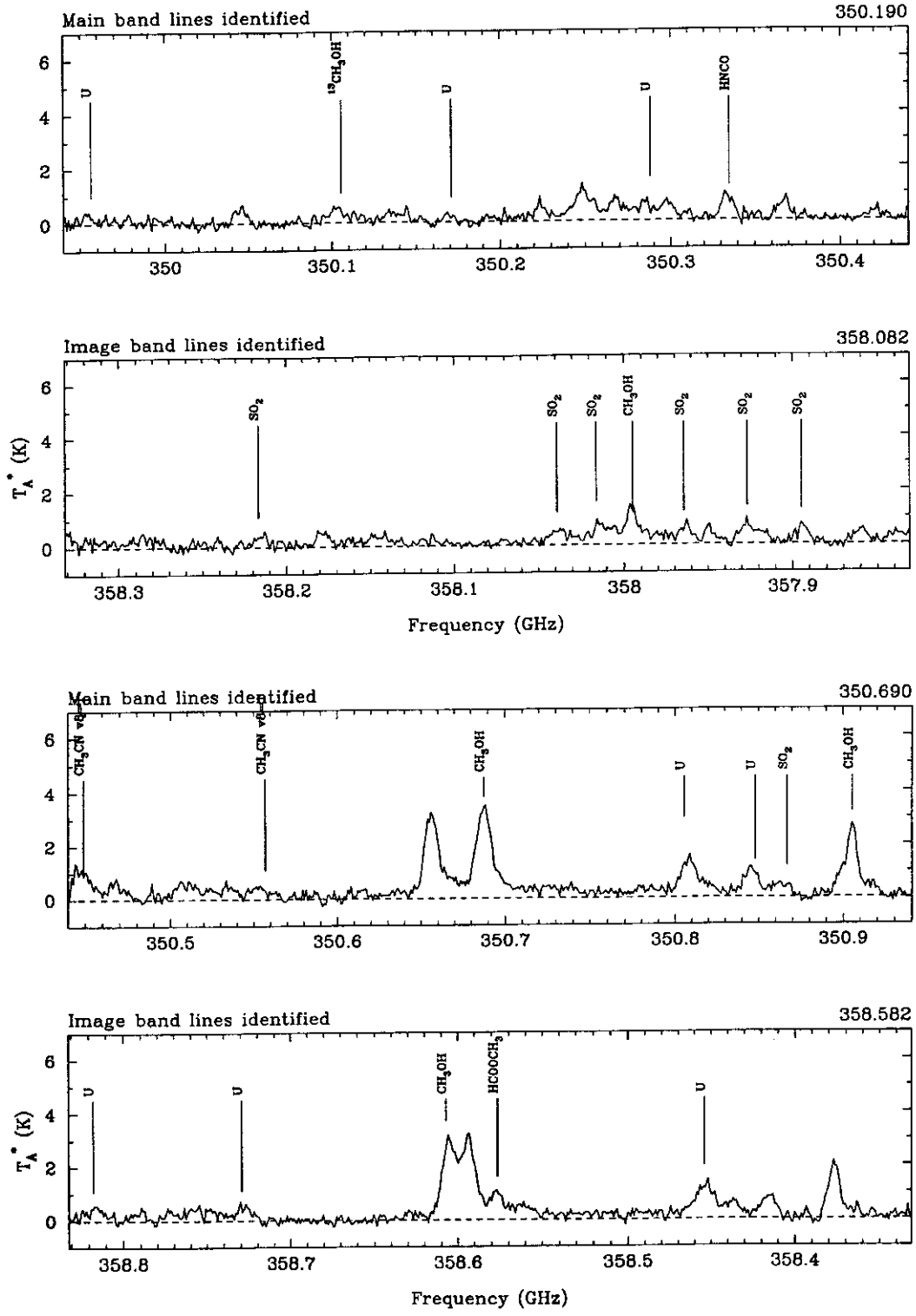

Fig. 4. continued

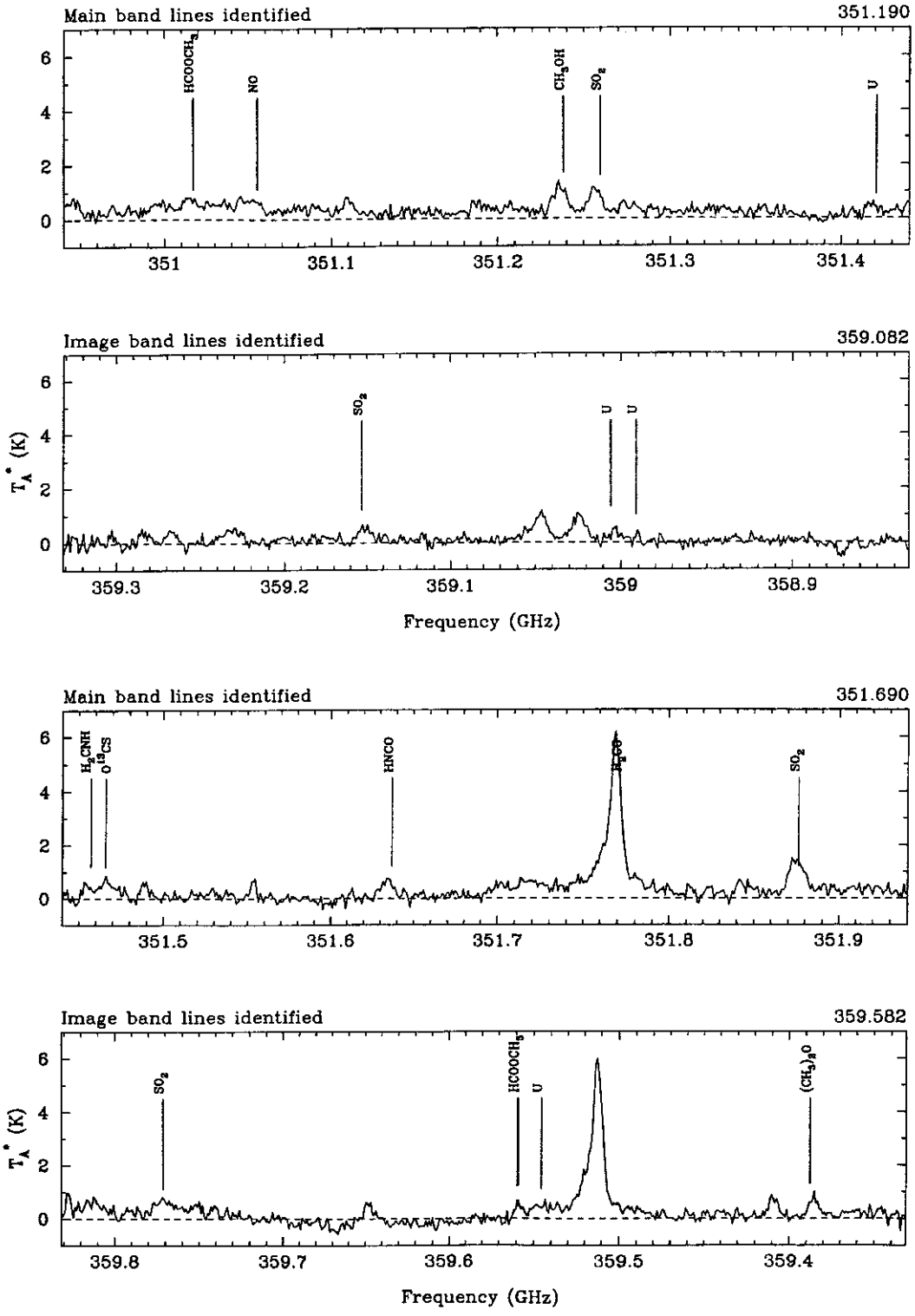

Fig. 4. continued

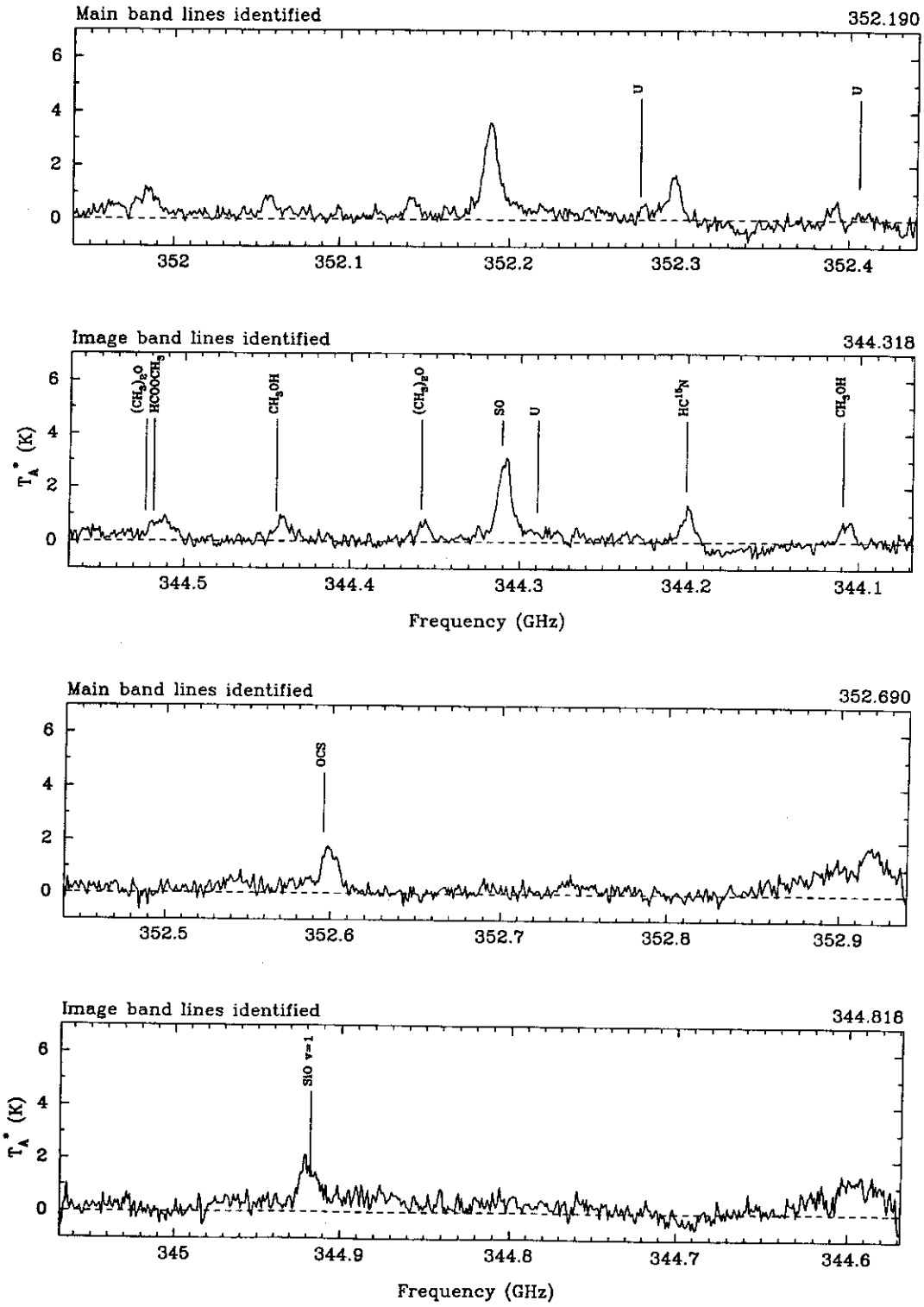

Fig. 4. continued

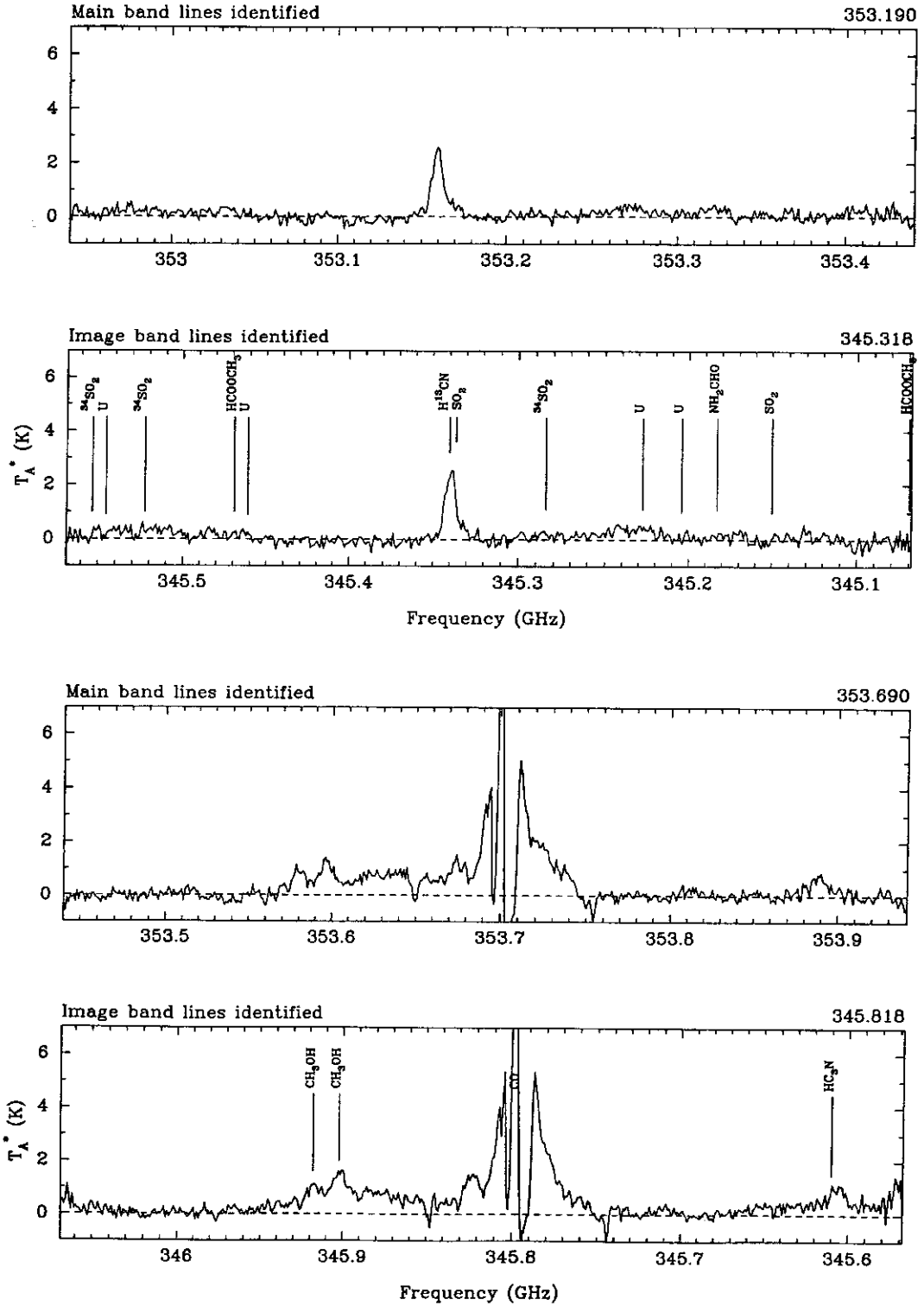

Fig. 4. continued

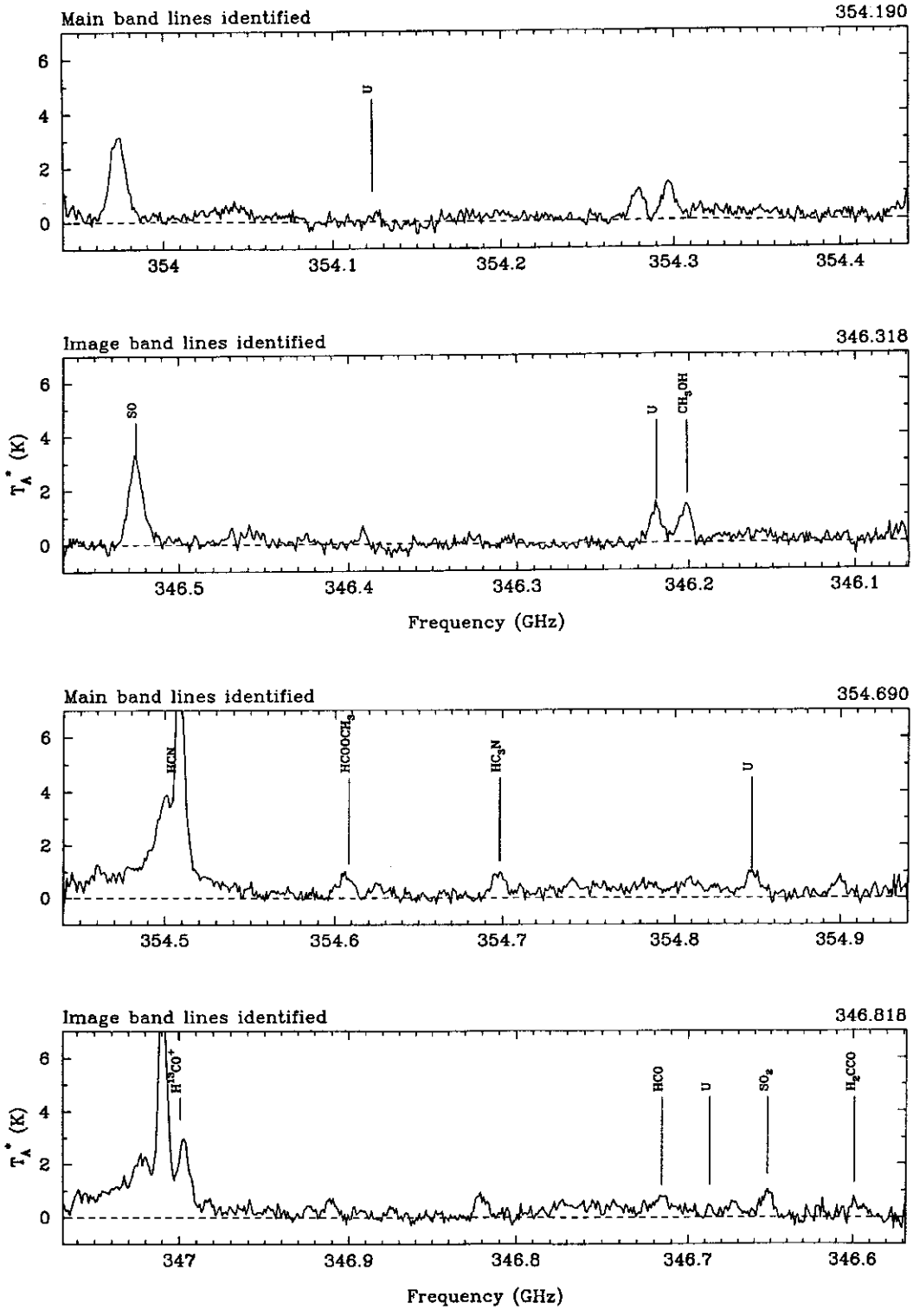

Fig. 4. continued

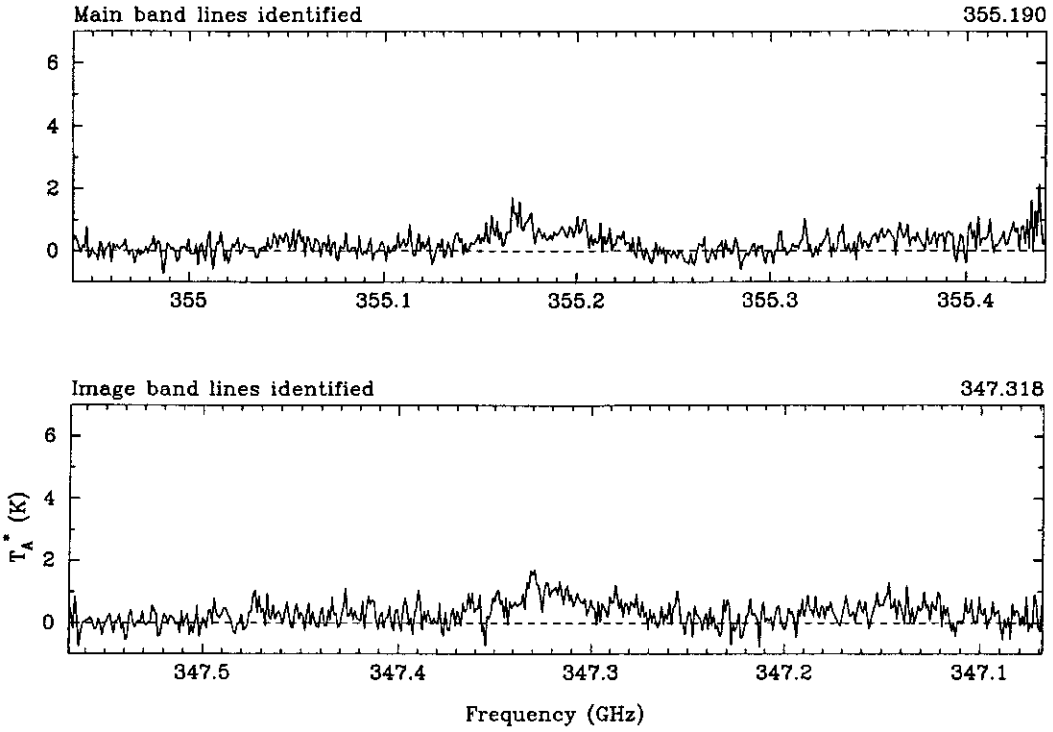

Fig. 4. continued